

Memory Loss and Auger Processes in a Many Body Theory of Charge Transfer

A.V. Onufriev and J. B. Marston

Department of Physics, Brown University, Providence, RI 02912-1843

(December 12, 1995)

cond-mat/9512102

Charge transfer between hyperthermal alkali atoms and metallic scattering surfaces is an experimental and theoretical arena for many-body interactions. To model new facets, we use a generalized time-dependent Newns-Anderson Hamiltonian which includes electron spin, multiple atomic orbitals with image shifted levels, intra-atomic Coulomb repulsion, and resonant exchange. A variational electronic many-body wave function solves the dynamical problem. The wave function consists of sectors with either zero or one particle-hole pair and goes beyond earlier work with the inclusion of amplitudes for a neutral atom plus an electron-hole pair. Higher order sectors with more than one particle-hole pair are suppressed by powers of $1/N$; hence the wave function ansatz is equivalent to a $1/N$ expansion. The equations of motion are integrated numerically without further approximation. The new solution shows improved loss-of-memory – the final charge state is independent of the initial one – in agreement with theoretical and experimental expectations. Understanding of this phenomenon is deepened through an analysis of entropy production. By studying the independent-particle approximation, and by examining the role played by different sectors of the Hilbert space in entropy production, we arrive at necessary and sufficient conditions for loss-of-memory to occur in the many-body solution. As further tests of the theory, we reproduce the experimentally observed peak in the excited neutral Li(2p) occupancy at intermediate work functions starting from different initial conditions. Next, we include Auger processes by adding two-body interaction terms to the many-body Hamiltonian. Several types of Auger processes are considered, and these are shown to affect the final state occupancies at low work-functions because phase space increases rapidly as the work-function is lowered. Preliminary experimental evidence for an upturn in the Li(2p) occupancy at the lowest work-functions thus may be explained by Auger transitions. Finally, we comment on the plausibility of observing a signature of the Kondo resonance in charge transfer experiments.

71.27.+a, 34.70.+e, 79.20Rf

I. INTRODUCTION

Charge-transfer between metallic surfaces and atoms is a quantum mechanical many-body phenomenon. Electrons of either spin up or spin down can neutralize a positive ion, but once one species has transferred to the atom, electrons of the opposing spin are blocked, at least partially, by the two-body Coulomb repulsion U . In previous work¹ [I] the time-dependent Newns-Anderson Hamiltonian was employed as a model of resonant charge transfer dynamics in the scattering of alkali atoms off metal surfaces. The only approximation made in solving the model was a systematic truncation of the Hilbert space. This variational approach, pioneered in the static case by Varma and Yafet², and in the dynamical problem by Brako and Newns³, is equivalent to a systematic $1/N$ expansion, where N is the spin degeneracy of the electrons which equals two for the physical case of spin up and down. The model and its approximate solution have been used by two experimental groups to describe the interaction of hyperthermal Li, Na, and K ions with an Alkali/Cu(001) surface⁴ and Li ions with an Alkali/Al(100) surface⁵. Qualitative agreement has been found between experiment and theory.

In this article we extend the many-body model of [I] by adding Auger processes. We also improve the approximate solution by including higher-order terms. One test of the accuracy of the approximation is provided by the phenomenon of loss-of-memory, which is said to occur when the final state of a dynamical system is independent of its initial state. It has been experimentally observed⁶ that the relative proportion of charge species in a scattered beam of atoms depends only on parameters such as surface work-function and the outgoing velocity. Loss-of-memory occurs in the independent-particle approximation to the many-body Newns-Anderson Hamiltonian⁷ and, as explained below, should also occur in better approximations which respect the strong intra-atomic correlation. To test loss-of-memory in the approximate solution we integrate the equations of motion forward in time starting from four different initial conditions. The calculations show a significant improvement of loss-of-memory compared to that found in [I] with a more restricted Hilbert space. By analyzing loss-of-memory in terms of the increase of entropy, we find a simple explanation for this improvement.

Loss-of-memory is important for another reason. The Newns-Anderson model breaks down when the atom is in the strong coupling region very close to the metal surface because the atomic orbitals, which in the model are assumed to be orthogonal to the metal states, hybridize with surface states. Nevertheless, as long as loss-of-memory occurs, the Newns-Anderson model will be an accurate description of charge transfer because the final charge state of the outgoing atom is determined on the outbound portion of its trajectory, beyond the strong coupling region. The breakdown in the model close to the surface therefore does not affect the subsequent physics of charge transfer further out.

The outline of the rest of the paper is as follows. In Sec. II we discuss the generalized Newns-Anderson Hamiltonian of resonant charge transfer. The approximate solution of the model is presented in Sec. III. To the Hilbert space originally considered in [I] we add new sectors to the many-body wave function at order $1/N$ which correspond to a neutral atom plus a particle-hole pair and solve the resulting equations of motions numerically. We compare the solutions to ones obtained previously in [I] and find that the new model agrees better with experiment as there is improved loss-of-memory. We also comment on the plausibility of observing the Kondo effect in charge transfer experiments. Sec. IV of the present work is devoted to analyzing the origin of loss-of-memory. We study the relationship between loss-of-memory and growth in a coarse-grained von Neumann entropy. For comparison, we also calculate the corresponding entropy increase in the independent-particle approximation. Since the Hilbert space is unrestricted in the independent-particle approximation, the comparison clarifies how the truncation of Hilbert space affects entropy production. In Sec. V we add two-body interaction terms to the original Hamiltonian which model several types of Auger processes. A simple phase-space argument shows that these couplings are increasingly important at low work-functions. We demonstrate that Auger processes can explain the experimentally observed⁸ upturn in the formation of excited Li(2p) atoms at the very lowest work-functions. Conclusions are presented in Sec. VI.

II. THE GENERALIZED NEWNS-ANDERSON MODEL

To model the dynamics of charge transfer, we make several simplifying assumptions. We employ the Newns-Anderson Hamiltonian, ignore radiative charge transfer processes, and for now consider only resonant charge transfer. The electrons in the target metal are modeled as zero-temperature non-interacting spinning fermions, albeit with the renormalized dispersion of a Landau Fermi liquid.⁹ The zero-temperature approximation is justified, as experiments typically operate at temperatures much less than other relevant electronic energy scales. The atom is modeled as a system with a finite number of discrete states moving along a fixed classical trajectory given by $z(t)$ where z is the distance from the atom to the metal surface. Each of these atomic states couples to the metal electrons when the atom is close to the metal surface. Feedback between the electronic degrees of freedom and the trajectory is ignored in the formulation. This trajectory approximation should be adequate as long as the kinetic energy of the ion is much larger than the electronic energies.

The model is defined by the following generalized time-dependent Newns-Anderson Hamiltonian:

$$\begin{aligned}
H(t) = & \sum_a [\epsilon_a^{(1)}(z)\hat{P}_1 + \epsilon_a^{(2)}(z)\hat{P}_2] c_a^{\dagger\sigma} c_{a\sigma} + \sum_k \epsilon_k c_k^{\dagger\sigma} c_{k\sigma} \\
& + N^{-1/2} \sum_{a; k} \{ [V_{a;k}^{(1)}(z)\hat{P}_1 + V_{a;k}^{(2)}(z)\hat{P}_2] c_a^{\dagger\sigma} c_{k\sigma} + H.c \} \\
& + \frac{1}{2} \sum_a U_{aa} n_a (n_a - 1) + \sum_{a>b} U_{ab} n_a n_b .
\end{aligned} \tag{1}$$

Here the fermion operator $c_a^{\dagger\sigma}$ creates a spin σ electron in orbital a of the atom. For Lithium, $a = 0$ for the 2s orbital, $a = 1, 2,$ and 3 for $2p_z, 2p_x,$ and $2p_y,$ etc. Likewise, $c_k^{\dagger\sigma}$ creates an electron of momentum k and energy ϵ_k in the metal. Of course, k is really a three-vector which labels all of the levels in the metal, both filled and empty, but it may be regarded as a scalar without loss of generality by absorbing the three-dimensional aspects of the problem into ϵ_k and $V_{a;k}$. We introduce the operators \hat{P}_1 and \hat{P}_2 to project respectively onto atoms with one or two valence electrons. These projectors, which may be written in terms of the orbital occupancies $n_a \equiv c_a^{\dagger\sigma} c_{a\sigma}$, permit one to assign different orbital energies, $\epsilon_a^{(1)}$ and $\epsilon_a^{(2)}$, and metal-atom couplings, $V_{a;k}^{(1)}$ and $V_{a;k}^{(2)}$, to the two cases of neutral atoms and negative ions. An implicit sum over repeated upper and lower Greek indices is adopted; for now $N = 2$ and $\sigma = 1, 2$ to represent the physical SU(2) case of spin up and down electrons. We have multiplied the atom-metal resonant coupling by a factor of $N^{-1/2}$. This factor keeps atomic level widths finite in the $N \rightarrow \infty$ limit. Finally, we eliminate excited negative ions from the Hilbert space by taking the Coulomb repulsion $U_{ab} \rightarrow \infty$ for $a, b \neq 0$.

The orbital energies and atom-metal couplings change with time. Time-dependence enters through the ion trajectory, which we model as:

$$\begin{aligned}
z(t) &= z_f - u_i * t; \quad t \leq t_{turn} \equiv (z_f - z_0)/u_i . \\
&= z_0 + u_f * (t - t_{turn}); \quad t > t_{turn}.
\end{aligned}
\tag{2}$$

Thus the trajectory starts at a distance z_f far away from the surface at time $t = 0$. We account roughly for the decrease in ion kinetic energy during impact, due principally to the recoil of surface atoms and the change in the scattering angle, by instantaneously changing the initial perpendicular component of the ion velocity, u_i , to $u_f < u_i$ at the point of closest approach, z_0 .

The Fermi energy ϵ_F is defined to be zero and the vacuum level lies above ϵ_F at work-function W . For simplicity, we define all orbital energies ϵ_a relative to ϵ_F . Because of image charges, the orbital energies of the neutral atom $\epsilon_a^{(1)}$ shift upward by $e^2/4z$ as the atom approaches the metal surface. To parametrize this z -dependence we use the following form for $\epsilon_a^{(1)}$ which saturates close to the surface:

$$\begin{aligned}
\epsilon_a^{(1)}(z) &= I_a + W + (1/v_{max}^2 + 16(z - z_{im})^2/e^4)^{-1/2}, \quad z > z_{im} \\
&= I_a + W + v_{max}, \quad z < z_{im}
\end{aligned}
\tag{3}$$

Here I_a is the ionization energy of an orbital a of an isolated atom which is taken to be negative and z_{im} is the distance from the surface at which the image shift saturates to the value v_{max} .

In contrast to the ionization levels, the affinity levels shift downward as the atom approaches the surface. In other words, the energy required to remove the two valence electrons bound to a negative alkali ion (thereby making it a positive ion) is unaffected by the image charges. As the intra-atomic Coulomb repulsion is already accounted for explicitly in the two-body interaction term in Eq. (1), the orbital energies for the negative ion are given by the same formula as Eq. (3) without the image shift:

$$\epsilon_a^{(2)} = I_a + W .
\tag{4}$$

The Coulomb energy between two electrons in the lowest s-orbital ($a = 0$) is then given by $U_{00} = A - I_0$ where A is the electron affinity (also defined here to be negative). The atom-metal couplings $V_{a,k}$ decay exponentially with distance when the atom is far from the metal surface because the atomic wave functions drop off exponentially with increasing distance from the atom, and the electronic wave functions in the metal fall off exponentially with increasing z . Closer in, the couplings deviate from the pure exponential form and saturate. In the following calculations we ignore the k dependence of the metal-atom coupling. This approximation is justified in so far as most of the resonant electronic processes occur close to the Fermi surface and the wave vector dependence of the couplings is smooth.

The metal states are labeled by $2M$ discrete momenta, M above the Fermi energy and M below it. We set $M = 30$ in the numerical calculations presented below, a sufficient number to sample the continuum of states accurately. Though the couplings $V_{a,k}$ are of fundamental importance in the many-body theory, it is convenient to express them in terms of the atomic half-widths, as the couplings must be rescaled each time we change the number of discrete metal states, M . We relate couplings and half-widths Δ_a via the approximate independent-particle Fermi Golden Rule formula:

$$V_{a;k}^2 = \frac{\Delta_a}{\pi\rho}
\tag{5}$$

where $\rho = M/D$ is the density of states for a flat band of half width D . Level half-widths $\Delta_a(z)$ are obtained from first principle calculations, within an independent-particle approximation, carried out by Nordlander and Tully¹⁰ and Nordlander¹¹. Exact values for $V_{a;k}$ will, of course, differ somewhat from those obtained via Eq. (5). To be useful, theoretical predictions must be robust to changes in the values of the couplings. A simple 3-parameter function, which accounts both for exponential decrease away from the surface and saturation close to it, fits the calculated widths well¹²:

$$\Delta_a(z) = \frac{\Delta_0}{[e^{4\alpha z} + (\Delta_0/\Delta_{sat})^4 - 1]^{1/4}} .
\tag{6}$$

To be concrete, we study the case of Lithium atoms interacting with a Cu(001) surface. Some of the parameters which appear in the Hamiltonian Eq. (1) via equations Eq. (2), Eq. (3), and Eq. (6) are fixed throughout the rest of the paper. In Eq. (2) we either start the trajectory far away from the surface at $z_f = 20\text{\AA}$ and bounce off the surface at $z_0 = 1\text{\AA}$ or begin from the point of closest approach, z_0 , and integrate outward. In Eq. (3) we take $z_{im} = 0.0\text{\AA}$ and $v_{max} = 2.6$ eV. For Lithium, the ionization energy from the 2s ground state is given by $I_0 = -5.39$ eV and the ionization energy from the $2p_z$ excited state is $I_1 = -3.54$ eV. We ignore the $2p_{x,y}$ states as they couple only weakly

to the metal. We also eliminate higher lying excited states and, as mentioned above, excited states of the negative ion as these states are not expected to become significantly populated. The electron affinity energy in Eq. (4) is given by $A = -0.62$ eV. Finally, the half-bandwidth of Copper is given approximately by $D = 4$ eV. Parameters appearing in the resonant widths formula Eq. (6) are given in Table I. Parameters which vary are the surface work-function W and the incoming and the outgoing velocities of the Lithium atom u_i and u_f . Values for these variables are listed in the text below and in the figure captions.

III. SYSTEMATIC SOLUTION

To construct an approximate wave function for the problem we follow Varma and Yafet² and also Brako and Newns³ and group the full many-body electronic wave function into sectors containing more and more numbers of particle-hole excitations in the metal. Upon truncating the wave function at a given number of particle-hole pairs, we obtain a variational wave function that spans only a small, but manageable, portion of the entire Hilbert space. The amplitude for particle-hole pair production is controlled at least formally by generalizing the two types of SU(2) electrons (spin up and down) to N types of SU(N) fermions. Thus the spin index σ now runs from 1 to N . We show below that the amplitudes for terms involving more and more particle-hole pairs are reduced by higher and higher powers of $1/N$.

To begin, we decompose the many-body wave function into five sectors, four of which were introduced in [I]. The new fifth sector consists of two parts, symmetric and antisymmetric. In this paper we adopt the convention of using capital letters to denote momenta indices which are restricted to values greater than k_F , or in other words, states above the Fermi energy. Lower case letters denote momenta indices which run over values less than k_F . The variational ansatz for the many-body wavefunction can then be written as:

$$\begin{aligned}
|\Psi(t)\rangle = & f(t)|0\rangle + \sum_{a; k < k_F} b_{a;k}(t)|a; k\rangle + \sum_{k < k_F, L > k_F} e_{L,k}(t)|L, k\rangle + \sum_{q < k < k_F} d_{k,q}(t)|k, q\rangle \\
& + \underbrace{\sum_{a; L > k_F, q < k < k_F} s_{a;L,k,q}(t)|a; L, k, q\rangle^S + \sum_{a; L > k_F, q < k < k_F} a_{a;L,k,q}(t)|a; L, k, q\rangle^A}_{\text{new sectors}} \\
& + (\text{rest of Hilbert space}) .
\end{aligned} \tag{7}$$

Each sector is a global SU(N) singlet. Non-singlet sectors can be ignored in so far as the initial state of the system, a closed shell positive alkali ion far away from an unperturbed non-magnetic metal, and the Hamiltonian are both SU(N) singlets. Here the orthonormal basis states in different sectors of the Hilbert space are given by:

$$\begin{aligned}
|a; k\rangle & \equiv N^{-1/2} c_a^{\dagger\sigma} c_{k\sigma} |0\rangle . \\
|L, k\rangle & \equiv N^{-1/2} c_L^{\dagger\sigma} c_{k\sigma} |0\rangle . \\
|k, q\rangle & \equiv [N(N-1)]^{-1/2} c_0^{\dagger\alpha} c_{k\alpha} c_0^{\dagger\beta} c_{q\beta} |0\rangle .
\end{aligned} \tag{8}$$

The basis for the new sectors is given by:

$$\begin{aligned}
|a; L, k, q\rangle^S & \equiv [2N(N-1)]^{-1/2} \{ c_L^{\dagger\alpha} c_{k\alpha} c_a^{\dagger\beta} c_{q\beta} |0\rangle + c_L^{\dagger\alpha} c_{q\alpha} c_a^{\dagger\beta} c_{k\beta} |0\rangle \} . \\
|a; L, k, q\rangle^A & \equiv [2N(N+1)]^{-1/2} \{ c_L^{\dagger\alpha} c_{k\alpha} c_a^{\dagger\beta} c_{q\beta} |0\rangle - c_L^{\dagger\alpha} c_{q\alpha} c_a^{\dagger\beta} c_{k\beta} |0\rangle \} .
\end{aligned} \tag{9}$$

The reference state $|0\rangle$ represents a positive alkali ion (i.e. an empty valence shell) along with the Landau Fermi-liquid at zero-temperature with no particle-hole excitations. According to the convention the limits on the momenta ranges appearing in Eqs. (8) and (9) are shorthand notation for $\epsilon_q < \epsilon_k < \epsilon_F$ and $\epsilon_L > \epsilon_F$ where $\epsilon_F \equiv 0$ is the Fermi energy. In other words, k and q label hole momenta, and L labels particle momentum, so while $|L, q\rangle$ is a positive ion plus a particle-hole pair, the state $|k, q\rangle$ instead represents a negative ion with two holes in the metal. A schematic of the different sectors of the Hilbert space is presented in Fig. 1. We show below that terms involving two or more particle-hole pairs constitute higher-order corrections which are dropped in the approximate solution.

The time-dependent coefficients appearing in the many-body wave function Eq. (7) are amplitudes for the following states:

- (1) $f(t)$ — A positive ion with no excitations in the metal, which is at absolute zero temperature. Note that $f(t=0) = 1$ describes the initial state of an experiment which directs incoming positive ions against the metal target.
- (2) $b_{a;k}(t)$ — A neutral atom with orbital a occupied and a hole left behind in the metal at momentum k .

(3) $e_{L,q}(t)$ — A positive ion and a single particle-hole pair in the metal (the electron has momentum L and the hole has momentum q).

(4) $d_{k,q}(t)$ — A negative ion with a double-occupied s-orbital ($a = 0$) and two holes in the metal at momenta k and q .

(5) $s_{a;L,k,q}$ and $a_{a;L,k,q}$ — Amplitudes for the new states which represent a neutral atom with orbital a occupied plus two holes in the metal with momenta k and q and a particle of momentum L . To enforce orthogonality, the sector is split into symmetric (s) and antisymmetric parts (a) with respect to interchange of momenta indices k and q . Physically, the state produced by an electron hopping to the atom from a metallic level k while another electron hops from q to L can be distinguished from the state in which k and q are interchanged. In the special case of no spin degeneracy $N = 1$, however, there is only one state, the antisymmetric one, as the particles are then spinless and can no longer be distinguished.

The logic behind the truncation scheme becomes clear upon considering the nature of the off-diagonal coupling, the terms in the Hamiltonian proportional to $N^{-1/2} V_{a;k}$. These terms couple adjacent sectors of the Hilbert space, as shown in Fig. 2. (By adjacent we mean sectors that differ by at most one elementary excitation in the band like a hole or a particle.) Repeated applications of the off-diagonal coupling to the reference state $|0\rangle$ generates all of the sectors in the singlet many-body wave function. Each time $V_{a;k}$ acts, it brings along a factor of $N^{-1/2}$. Thus amplitudes for sectors involving multiple particle-hole pairs are weakly coupled to lower order terms when N is large. In particular, from Eq. (10) below it is clear that the amplitudes of sectors containing a single particle-hole pair ($e_{L,q}$, $s_{a;L,k,q}$ and $a_{a;L,k,q}$) are reduced by a factor of $N^{-1/2}$ in comparison to the amplitudes for the sectors with no particle-hole pairs (f , $b_{a;k}$ and $d_{k,q}$). The probability for a particle-hole pair is therefore reduced by a factor of $1/N$. The restriction to this trial basis is achieved by projecting the Schrödinger equation $i\frac{d}{dt}\Psi = \hat{H}\Psi$ onto each sector of the Hilbert space to obtain the equations of motion. Following [I], to reduce computational work we remove diagonal terms from the equations of motion by a change of variables: $\lambda(t) = \Lambda(t)\exp^{-i\phi(t)}$ where $\lambda(t)$ is an amplitude and $\phi(t)$ would be the phase of the corresponding state were the coupling of the atom to the surface turned off. For instance, in the newly added sector, diagonalization is accomplished with the following change of variables:

$$\begin{aligned} s_{a;L,k,q}(t) &= S_{a;L,k,q}(t) \exp\{-i[\phi_a(t) + (\epsilon_L - \epsilon_k - \epsilon_q)t]\} \\ a_{a;L,k,q}(t) &= A_{a;L,k,q}(t) \exp\{-i[\phi_a(t) + (\epsilon_L - \epsilon_k - \epsilon_q)t]\} \end{aligned}$$

where $\phi_a(t) \equiv \int_0^t \epsilon_a^{(1)}(t') dt'$ is the time-evolved phase for the decoupled, but image-shifted, atomic orbital a . The resulting equations of motion are:

$$\begin{aligned} i\frac{d}{dt}F &= \sum_{a;k} V_{a;k}^{(1)*} \exp\{i[\epsilon_k t - \phi_a(t)]\} B_{a;k} . \\ i\frac{d}{dt}B_{a;k} &= V_{a;k}^{(1)} \exp\{i[\phi_a(t) - \epsilon_k t]\} F \\ &\quad + \delta_{a,0} \sqrt{1-1/N} \sum_q V_{0;q}^{(2)*} \exp\{-i[(U - \epsilon_q + 2\epsilon_0^{(2)})t - \phi_0(t)]\} [\theta(k-q) D_{kq} + \theta(q-k) D_{qk}] \\ &\quad + N^{-1/2} \sum_L V_{a;L}^{(1)} \exp\{i[\phi_a(t) - \epsilon_L t]\} E_{Lk} . \\ i\frac{d}{dt}E_{Lk} &= N^{-1/2} \sum_a V_{a;L}^{(1)*} \exp\{i[\epsilon_L t - \phi_a(t)]\} B_{a;k} \\ &\quad + \sqrt{(N-1)/2N} \sum_{a;q} V_{a;q}^{(1)*} \exp\{i[\epsilon_q t - \phi_a(t)]\} [\theta(k-q) S_{a;Lkq} + \theta(q-k) S_{a;Lqk}] \\ &\quad + \sqrt{(N+1)/2N} \sum_{a;q} V_{a;q}^{(1)*} \exp\{i[\epsilon_q t - \phi_a(t)]\} [\theta(k-q) A_{a;Lkq} - \theta(q-k) A_{a;Lqk}] . \\ i\frac{d}{dt}D_{kq} &= \sqrt{1-1/N} V_{0;q}^{(2)} \exp\{i[(U - \epsilon_q + 2\epsilon_0^{(2)})t - \phi_0(t)]\} B_{0;k} \\ &\quad + \sqrt{1-1/N} V_{0;k}^{(2)} \exp\{i[(U - \epsilon_k + 2\epsilon_0^{(2)})t - \phi_0(t)]\} B_{0;k} \\ &\quad + (2/N)^{1/2} \sum_L V_{0;L}^{(2)} \exp\{i[(U - \epsilon_L + 2\epsilon_0^{(2)})t - \phi_0(t)]\} S_{0;Lkq} . \\ i\frac{d}{dt}S_{a;Lkq} &= \delta_{a,0} (2/N)^{1/2} V_{0;L}^{(2)*} \exp\{-i[(U - \epsilon_L + 2\epsilon_0^{(2)})t - \phi_0(t)]\} D_{kq} \end{aligned}$$

$$\begin{aligned}
& + \sqrt{(N-1)/2N} [V_{a;q}^{(1)} \exp\{i[\phi_a(t) - \epsilon_q t]\} E_{Lk} + V_{a;k}^{(1)} \exp\{i[\phi_a(t) - \epsilon_k t]\} E_{Lq}] . \\
i \frac{d}{dt} A_{a;Lkq} & = \sqrt{(N+1)/2N} [V_{a;q}^{(1)} \exp\{i[\phi_a(t) - \epsilon_q t]\} E_{Lk} - V_{a;k}^{(1)} \exp\{i[\phi_a(t) - \epsilon_k t]\} E_{Lq}] .
\end{aligned} \tag{10}$$

In the above equations we have used the following symmetries of the amplitudes: $D_{kq} = D_{qk}$, $S_{a;Lkq} = S_{a;Lqk}$, and $A_{a;Lkq} = -A_{a;Lqk}$. Also, we have corrected several typographical errors which appeared in Eq. (3.6) of [I]. As the amplitudes undergo unitary evolution forward in time, the sum of their squares is conserved and equals one.

The equations of motion are numerically integrated forward in time with the use of a fourth-order Runge-Kutta algorithm with adaptive time steps. The double-precision C-code is run on IBM RS/6000 machines and, in a multi-processor form, on a Cray EL-98 computer.¹⁴ Probability is conserved to better than one part in 10^6 . For $M = 30$ levels, one run at a typical velocity takes on the order of ten minutes of RS/6000 CPU time. We choose one of the following four initial conditions:

- (1) – A positive alkali ion A^+ far away ($z = z_f$) from the surface. The only nonzero initial amplitude is $F(t=0) = 1$.
- (2) – A neutral, unexcited, alkali atom A^0 far away. The only nonzero initial amplitude is $B_{0,0} = 1$. A single hole lies at the Fermi energy.
- (3) – A negative alkali ion A^- far away. The only nonzero initial amplitude is $D_{0,0} = 1$. Two holes lie at the Fermi energy.
- (4) – Start at the point of closest approach, $z = z_0$, in the equilibrium ground state. (The ground state is obtained via the imaginary-time Lanczos algorithm.) This initial condition is realized in sputtering experiments.

In Fig. 4(a) we present results from the improved equations of motion for the case of a Lithium atom striking a clean Cu(001) surface of work-function $W = 4.59$ eV for three different initial conditions, (1), (2), and (4), and over a range of velocities (0.005 a.u. $< u_f < 0.05$ a.u.). The occupancies change by less than 1% when the number of metal levels below the Fermi energy, M , is increased from 30 to 60. For comparison, in Fig. 4(b) we also report results obtained from the previous equations of motion of [I] which are missing the new sectors. Note in particular the significant improvement in loss-of-memory compared to that found in [I] for all three initial conditions. From both experiment^{6,12} and the independent-particle approximation¹³, we expect loss-of-memory to be complete at this velocity. Evidently the systematic $1/N$ expansion works better and better as the Hilbert space is enlarged and higher order terms are included. However, we also find that loss-of-memory is absent from both solutions for initial condition (3), the negative ion. For this initial condition, the final charge state is nearly 100% neutral (A^0) for the improved equations of motion, and 100% negative (A^-) in the case of [I]. The breakdown of loss-of-memory for the negative ion initial condition has an explanation in the particular manner in which the Hilbert space is truncated, and we return to this question below in Sec. IV.

Another important test of the improved approximation is whether it reproduces the peak in the excited neutral Li(2p) occupancy seen in experiments^{1,8} at a surface work-function value of $W \approx 2.8$ eV. The improved calculations, like those reported previously in [I], do in fact yield a peak. (The physical origin of this peak is discussed in Sec. V below.) Experimental measurements⁸ of the number of photons produced by the decay of the excited Li(2p) state to Li(2s) are plotted alongside the calculated final Li(2p) occupancy in Fig. 3 for the case of initial conditions (2) and (4). Good qualitative agreement between theory and experiment is obtained. The positive ion initial condition does not, however, yield results which agree with experiment at the work-functions below 2.8 eV as the Li(2p) occupancy continues to grow monotonically. We attribute the breakdown at low work-functions to the truncation of the Hilbert space. A term at order $1/N$ has been left out because it has four momenta indices: the amplitude in the A^- sector corresponding to a negative ion with two holes plus a particle-hole pair in the metal. We expect that this term could absorb the excess excited neutrals at low work-functions.

Scattering experiments off clean surfaces are the best arena for answering quantitative questions about many-body effects, as complications involving surface adsorbates are then avoided. Recently Shao *et al.* have made an interesting suggestion: at low velocities, a Kondo resonance should appear in the atomic spectral function.¹⁵ To argue that this resonance could be observable in charge-transfer experiments, Shao *et al.* employ a slave boson non-crossing approximation (NCA) treatment of the time-dependent Newns-Anderson model¹⁶. Shao *et al.* argue, based on an assumed pure exponential form for the atom-metal coupling, that the Kondo peak could show up as deviations from a single straight line in a plot of the logarithm of the atomic occupancy versus the inverse perpendicular velocity.

It is important to note that the slave boson NCA approximation breaks down when the atom is in a mixed valence state, which must occur whenever there is a level crossing the Fermi energy. In particular, a nonphysical temperature scale appears within NCA. It is an artifact of the approximations made: especially, the neglect of vertex corrections.¹⁷ Away from a level crossing it is small and can usually be neglected. This is no longer the case in charge transfer experiments, where the Kondo temperature is of order $\sqrt{D\Delta}$ near the level crossing. Then the unphysical temperature scale is of order D^2/Δ which is generally larger than both the bandwidth, D , and the Kondo temperature¹⁷. A comparison between the NCA approximation and an essentially exact renormalization group (RG) analysis of the Anderson impurity model also shows that NCA is an inaccurate approximation for dynamical properties.¹⁸ In contrast

the $1/N$ approximation employed here is free of these difficulties as it contains vertex corrections. For example, the Kondo peak disappears in the variational $1/N$ approach at $N = 1$ as it should, since there is no longer any spin degeneracy. In the slave boson NCA approximation it persists as an unphysical feature.¹⁷

Besides the technical limitation of the slave boson NCA approximation, other problems arise in attempting to extract the weak Kondo signal from the large background. Shao *et al.* assume that the negative ion has the same width as the neutral¹⁵ but this assumption should be relaxed since, as noted above, negative alkali ions are larger than neutral atoms. This means negative ion yields cannot be directly compared to positive yields. Furthermore, the detailed form of the width is not a pure exponential and this may introduce additional non-linearities which will be difficult to separate from those produced by the Kondo resonance. Excited states also have been neglected in the model of Shao *et al.*, but these may cause wiggles in the occupancy which could be misinterpreted as Kondo effects. Indeed, we find no clear signature of the Kondo resonance in the approximate solution to our model, which incorporates these generalizations. Finally, there appears to be no way to do a control experiment in which only the intra-atomic Coulomb repulsion is turned off, with all else left unchanged. Nevertheless, the observation that Kondo effects can in principle occur serves to underscore the many-body nature of charge-transfer.

IV. ORIGIN OF MEMORY LOSS

In this section we analyze how the $1/N$ expansion works in the dynamical problem. In particular, we investigate the physical mechanism responsible for loss-of-memory. We analyze how loss-of-memory is affected by the truncation of the Hilbert space to clarify why the approximate solution exhibits loss-of-memory for three of the four initial conditions while it breaks down for the case of an incoming negative alkali ion. We begin by formulating a simple necessary criterion for memory loss to occur and show that it is always satisfied as long as the initial velocity of the atom is low enough. As loss-of-memory is not complete in the approximate solution, we conclude that the conditions which determine its presence or absence are more subtle. To characterize the phase decoherence of the initial state and thus loss-of-memory, we introduce a coarse-grained entropy in both the independent-particle and in the many-body pictures. In the former case the Hilbert space is unrestricted and loss-of-memory at low velocities is complete¹⁹. By comparing entropy increase in the two pictures we gain insight into the importance of the higher-order sectors left out in the truncated Hilbert space of Eq. (7). We show that the probability flow between different sectors of the Hilbert space is toward the direction of increasing entropy; the entropy grows as probability flows to sectors which occupy larger and larger portions of phase space.

First we review the phenomenon of loss-of-memory within the independent particle approximation. In this approximation, we neglect the strong correlations between electrons on the atom by reducing the atomic states to a single orbital, and by treating the electrons as spinless ($N = 1$). Then the Pauli exclusion principle, instead of the intra-atomic Coulomb repulsion, prevents multiple occupancy of the atomic orbital. Consider an atom initially in some state $|a\rangle$ incident on the metal surface. As the atom moves towards the surface, it begins to forget its initial state. If the atom does not spend enough time close to the surface, however, the initial state will not decay completely, and the final charge state will depend on the initial one. Thus the atom must move slowly enough for loss-of-memory to occur. In the independent-particle approximation, for the case of infinite bandwidth ($D \rightarrow \infty$), the following expression is obtained for the time-evolution of the expected atomic occupancy¹⁹:

$$n_a(t) = n_a(0) \exp\left(-2 \int_0^t \Delta[z(t')] dt'\right) + O(t) . \quad (11)$$

The first term is the memory term n_a^{mem} which depends on the initial atomic occupancy $n_a(0)$. The second term $O(t)$ does not interest us here as it is independent of the initial condition. Assuming pure exponential dependence of the level width on distance, $\Delta(z) \equiv \Delta_0 \exp(-\alpha z)$, and using the trajectory approximation Eq. (2), the memory term in (11) may be rewritten along the inward bound portion of the trajectory as:

$$n_a^{mem}(t) = n_a(0) \exp\left(-\frac{2\Delta_0}{\alpha u_i} \exp[-\alpha(z_f - u_i t)]\right) . \quad (12)$$

Initially the atom is at a distance z_f from the surface and moves towards it with a velocity u_i . It reaches the surface at $t = t_{turn} = z_f/u_i$ and loss-of-memory is thus complete if $n_a^{mem}(t_{turn}) \ll n_a(0)$ or in other words,

$$2\Delta_0 \gg \alpha u_i . \quad (13)$$

The physical meaning of this equation is that there must be enough time for an electron to hop back and forth between the atom and the metal several times for loss-of-memory to be complete. Parameters for the half-widths of Lithium are

given in Table I. For the 2s orbital, $\Delta_0 = 2.23$ and $\alpha = 0.86$. Thus at a typical incoming velocity of $u_i = 0.04$ a.u., Eq. (13) is well satisfied. Although the above estimate is based on the independent-particle approximation and assumes a pure exponential form for $\Delta(z)$, the conclusion is valid in the many-body case and for the more general form for $\Delta(z)$ we use below, as the key physical feature, the coupling of the atomic level to a continuum of states in the metal, is unchanged. Indeed, loss-of-memory occurs within the slave boson NCA approximate solution to the dynamical many-body problem in which a class of bubble diagrams is summed to all orders.¹⁶ In a low-velocity limit the slave boson NCA approximation reduces to a set of first-order rate equations which necessarily exhibit loss-of-memory whenever the occupancy of any channel attains unity along the trajectory. However, as quantum mechanical phase information is thrown away in the semiclassical rate equations, they are inaccurate at velocities of most experimental interest^{13,20} and we do not consider them further here.

It is useful to examine the time evolution of an atom held at a fixed position close to the surface as the Hamiltonian is then time-independent. If there is no loss-of-memory for different initial conditions, then loss-of-memory will, in general, be absent in the dynamical problem. Results for the approximate solution to the many-body problem are presented in Fig. 5. It typically takes $\tau_i \approx 10^{-15}$ sec for the occupancies to settle down to constant values. This interaction time scale is shorter than the typical amount of time the atom spends in the region of strong coupling in the dynamical problem, $\tau_m > 5\text{\AA}/0.05a.u. \approx 5 \times 10^{-15}$ sec. Small oscillations in the occupancies with period 1.03×10^{-15} sec at large time are due to the finite metal bandwidth, $D = 4eV$, and are washed out in the dynamical system. The occupancies change by less than 0.1% when the number of metal states above or below the Fermi energy, M , is increased from 30 to 60. Note that Poincaré recurrence, relevant when the coupling between the atom and the surface is weak, occurs at the longer time $\tau_r = 2\pi\hbar M/D \approx 2 \times 10^{-14}$ sec and can be ignored. The final atomic occupancies of about 80% positive fraction are nearly the same for three of the initial conditions - positive ion (1), neutral atom (2), and equilibrium ground state (4). In the case of the negative ion initial condition (3), however, the final charge state is mostly neutral, not positive.

Study of the effects of the truncation of the Hilbert space on loss-of-memory in the many-body solution requires a quantitative measure of decoherence. For this purpose we may introduce the fine-grained quantum mechanical von Neumann entropy, $S_{fg}(t) \equiv -Tr\{\hat{\rho}(t) \ln \hat{\rho}(t)\}$, where $\hat{\rho}(t)$ is the density matrix. The fine-grained entropy, however, is constant for any time-independent Hamiltonian as no phase information is lost in a system undergoing unitary time evolution. Thus, $\rho(t) = \hat{U}(t)\hat{\rho}(0)\hat{U}^\dagger(t)$ where $\hat{U}(t) = \exp(-i\hat{H}t)$, so $S_{fg}(t) = -Tr\{\hat{U}(t)\hat{\rho}(0)\hat{U}^\dagger(t)\hat{U}(t) \ln \hat{\rho}(0)\hat{U}^\dagger(t)\}$. Grouping together $\hat{U}(t)$ and $\hat{U}^\dagger(t)$ under the Tr symbol, it is straightforward to see that $S_{fg}(t) = -Tr\{\hat{\rho}(0) \ln \hat{\rho}(0)\} = S_{fg}(0)$. Instead, we coarse-grain²¹ the system by ignoring information contained in the off-diagonal matrix elements of $\hat{\rho}$. The coarse-grained entropy is then defined to be:

$$S_{cg}(t) = - \sum_a \rho_{aa}(t) \ln \rho_{aa}(t) \quad (14)$$

where ρ_{aa} are the diagonal matrix elements of $\hat{\rho}$ which time evolve as:

$$\rho_{aa}(t) = \sum_b |U_{ab}(t)|^2 \rho_{bb}(0) + \sum_{b \neq c} U_{ab}^*(t) U_{ac}(t) \rho_{bc}(0) . \quad (15)$$

The second term in this equation contains all the information about phase correlations, and we expect it to vanish in the $t \rightarrow \infty$ limit provided the Hilbert space is large enough. Then it is easy to show²¹ that $dS_{cg}(t)/dt \geq 0$, the quantum mechanical analogue of the Boltzmann H-theorem.

It is straightforward to compute the coarse-grained entropy Eq. (14) from the many-body states Eq. (7):

$$\begin{aligned} S_{cg}(t) = & -|F|^2 \ln |F|^2 - \sum_{a;k} |B_{ak}|^2 \ln |B_{ak}|^2 - \sum_{L,k} |E_{Lk}|^2 \ln |E_{Lk}|^2 - \sum_{k>q} |D_{kq}|^2 \ln |D_{kq}|^2 \\ & - \sum_{a;L,k>q} |S_{a;Lkq}|^2 \ln |S_{a;Lkq}|^2 - \sum_{a;L,k>q} |A_{a;Lkq}|^2 \ln |A_{a;Lkq}|^2 - \dots \end{aligned} \quad (16)$$

where the ellipses denote contributions from higher order sectors not included in the variational wavefunction. In the independent-particle picture the coarse-grained entropy is given by the standard expression for the statistical mechanical entropy²²:

$$S_{cg}(t) = - \sum_k n_k \ln n_k - \sum_k (1 - n_k) \ln(1 - n_k) - n_a \ln n_a - (1 - n_a) \ln(1 - n_a) . \quad (17)$$

Here n_k is the occupancy of the metal band level k and n_a is the atomic occupancy. It is important to note that the two entropy definitions, Eqs. (16) and (17), are not exactly equivalent, even for the case of spinless electrons.

Information in the form of two-body and higher order correlations contained in Eq. (16) has been thrown away in Eq. (17) where only the one-body occupancies appear. For example, each Hilbert space sector of Eqs. (8) and (9) strictly conserves total particle number. Conservation of total particle number is reflected in non-trivial two-body correlations which are discarded when the state is described purely in terms of one-body occupancies. While the two entropies are equal in the limit of a macroscopic number of excitations, for the finite number of excitations generated in an atom-surface collision the coarse-grained entropy of Eq. (17) is somewhat larger than that of Eq. (16).

Occupancies in the independent-particle approximation are obtained by solving equations of motion for the *operators* $\hat{c}_a(t)$ and $\hat{c}_k(t)$ as opposed to equations of motion for *amplitudes* like Eq. (10). To highlight this difference, we place hats on top of the operators. As there is no many-body interaction U in the independent-particle approximation, the Heisenberg equations of motion for the operators, obtained from Eq. (1), are linear:

$$\begin{aligned} i \frac{d}{dt} \hat{c}_a &= \epsilon_a^{(1)}(t) \hat{c}_a + \sum_k V_{0;k}^{(1)}(t) \hat{c}_k , \\ i \frac{d}{dt} \hat{c}_k &= \epsilon_k \hat{c}_k + V_{0;k}^{(1)}(t) \hat{c}_a . \end{aligned} \quad (18)$$

Here and below $a = 0$ and the momentum index k runs over all momenta, not just $k < k_F$. The operators at time t may be expressed as a linear combination of the operators at the initial time $t = 0$:

$$\begin{aligned} \hat{c}_a(t) &= f(t) \hat{c}_a(0) + \sum_k b_k(t) \hat{c}_k(0) , \\ \hat{c}_k(t) &= d_k(t) \hat{c}_a(0) + \sum_q e_{kq}(t) \hat{c}_q(0) . \end{aligned} \quad (19)$$

Initially, the time-dependent c-number coefficients are given by $f(0) = 1$, $b_k(0) = d_k(0) = 0$, and $e_{kq}(0) = \delta_{kq}$. Subsequent values are obtained from the equations of motion for the coefficients:

$$\begin{aligned} i \frac{d}{dt} f &= \epsilon_a^{(1)}(t) f + \sum_k V_{0;k}^{(1)}(t) d_k , \\ i \frac{d}{dt} b_k &= \epsilon_a^{(1)}(t) b_k + \sum_q V_{0;q}^{(1)}(t) e_{qk} , \\ i \frac{d}{dt} d_k &= \epsilon_k d_k + V_{0;k}^{(1)}(t) f , \\ i \frac{d}{dt} e_{kq} &= \epsilon_k e_{kq} + V_{0;k}^{(1)}(t) b_q . \end{aligned} \quad (20)$$

Once the diagonal terms are removed by a change of variables as in Eq. (10), these equations are numerically integrated forward in time with the fourth-order Runge-Kutta algorithm.¹⁴ The occupancies $n_a(t) = \langle \hat{c}_a^\dagger(t) \hat{c}_a(t) \rangle$ and $n_k(t) = \langle \hat{c}_k^\dagger(t) \hat{c}_k(t) \rangle$ may then be calculated for any initial state of the system. For example, in the case of an incident positive alkali ion and a filled Fermi sea, initially $n_a(0) = 0$ and $n_k(0) = 1$ for $k < k_F$. The many-electron wavefunction is then given at all times by the Slater determinant

$$|\Psi(t)\rangle = \prod_{k < k_F} \hat{c}_k^\dagger(t) |0\rangle = \prod_{k < k_F} [d_k^*(t) \hat{c}_a^\dagger(0) + \sum_q e_{kq}^*(t) \hat{c}_q^\dagger(0)] |0\rangle ; \quad (21)$$

here $|0\rangle$ is the true vacuum state devoid of any electrons. Now it is clear how an arbitrary number of particle-hole excitations are accommodated within the independent-particle approximation. From Eq. (21) it follows that $n_a(t) = \sum_{k < k_F} |b_k(t)|^2$, and $n_k(t) = \sum_{q < k_F} |e_{kq}(t)|^2$.

In Fig. 6 we plot the time evolution of the entropy in the independent-particle approximation and in the approximate solution to many-body model for the case of spinless fermions ($N = 1$) with and without the new sectors $|a; L, k, q\rangle$ of the Hilbert space, Eq. (7). We also eliminate excited atomic states in the many-body equations of motion Eq. (10) to permit direct comparison of the approximate many-body solution with the independent-particle solution. The initial state of the Lithium atom, which is held at fixed position $z = z_0 = 1.0\text{\AA}$, is a positive ion and the entropy is zero. As time advances, this pure state evolves into a mixed one and the entropy grows. Several features shown in Fig. 6 are generic for all of the initial conditions and parameters we tested. First, the entropy increase in the independent-particle case is comparable to that in the many-body case, even though the Hilbert space of the independent-particle solution is unrestricted. This suggests that sectors containing two and more particle-hole pairs, the ones not present in

the variational wavefunction, do not become significantly populated and can be safely neglected. Indeed the number of electron-hole pairs produced during a collision, estimated in the independent-particle solution by counting the expected number of particles due to pairs, $\sum_{k>k_F} n_k$, is typically less than one. Evidently an infrared catastrophe is avoided: the number of very low energy excitations is severely limited. We also see that entropy does not grow monotonically when the $|a; L, k, q\rangle$ sectors are dropped as the Hilbert space is now too restricted for phase decoherence to be complete. Finally, Fig. 7 shows how the entropy grows monotonically in the many-body solution for the physical case of spinning electrons, $N = 2$, with both excited neutral and negative ion states now included.

Entropy growth provides clues as to how probability flows between different sectors within the truncated Hilbert space. We again turn off the couplings to the negative ion and excited state sectors. The coarse-grained entropy grows in time as long as the Hamiltonian is time-independent. The main direction of the probability flow corresponds to flow into sectors with larger and larger phase space. The phase space corresponding to $|0\rangle$ is a single state and is therefore smaller than the phase space of the $|a; k\rangle$ sector which contains M states. The $|L, k\rangle$ sector occupies an even larger portion of the phase space consisting of M^2 states. Finally, sector $|a; L, k, q\rangle$ occupies the largest portion of the Hilbert space as it comprises M^3 states. Thus, probability which flows in the direction $|0\rangle \rightarrow |a; k\rangle$, $|a; k\rangle \rightarrow |L, k\rangle$, and $|L, k\rangle \rightarrow |a; L, k, q\rangle$ as shown in Fig. 8(a) leads to entropy increase while a reversal of flow would, in general, lead to a decrease of entropy and is improbable. As an illustration of probability flow, consider the time dependence of the occupancies shown in Fig. 9(a). The initial positive ion $|0\rangle$ state first dwindles into a group of neutral $|a; k\rangle$ states because in this case the surface work-function has been set to the low value of $W = 1.59$ eV. Later on, the higher order $|L, k\rangle$ and $|a; L, k, q\rangle$ sectors become partially populated. Had the initial state been a neutral atom and had the surface work-function been high, probability would instead have flowed from the single $|a; k = 0\rangle$ state diagonally into the ionized states with a particle-hole pair, $|L, k\rangle$. The alternative ionization route $|a; k = 0\rangle \rightarrow |0\rangle$ does not increase the entropy and is negligible compared to the $|a; k\rangle \rightarrow |L, k\rangle$ route. The approximate solution confirms this scenario in this case as the particle-hole sector $|L, k\rangle$ dominates the final A^+ occupancy.

An important feature of the probability cascade is the increasing time scale at which higher-order sectors become populated as seen for instance in Fig. 9(b). The atomic occupancies essentially reach their final values at $t = 7.5 \times 10^{-16}$ sec, despite the fact that probability continues to flow from $|0\rangle$ to $|L, k\rangle$ and from $|a; k\rangle$ to $|a; L, k, q\rangle$ even at much later times $t = 20 \times 10^{-16}$ sec. That the occupancy of the atomic orbital is unaffected by these subsequent probability flows to the higher-order sectors supports the use of the $1/N$ expansion, as the neglect of terms of order $1/N^2$ and higher should not significantly disturb observables accessible to experiment.

We next switch back on the coupling to A^- as depicted in Fig. 8(b). It is now clear why loss-of-memory breaks down for the A^- initial condition at high work-functions, as shown for instance in Fig. 5(c). For high work-functions the final charge state should be mostly A^+ . However, as shown in Fig. 8(b), there is no path of strictly growing entropy which leads from A^- into any of the sectors corresponding to A^+ . The probability can only flow into the $|a; L, k, q\rangle$ sector corresponding to a neutral atom and a particle-hole excitation, and stay there as in Fig. 5(c). We conjecture that loss-of-memory for this initial condition can be restored with the inclusion of a new sector corresponding to a positive ion with two particle-hole pairs, which appears at second order in $1/N$ as shown in Fig. 8(b). The probability may then cascade diagonally down from A^- to A^+ with increasing entropy at each step. The reason this sector has not been included is pragmatic: it is labeled by four momenta indices, and the computational power required to solve $O(M^4)$ differential equations versus $O(M^3)$ at the current level of approximation would be excessive.

Up until now we have focused on the static problem of an atom at fixed distance from the surface. We now return to the dynamical problem. Consider the positive ion initial condition (1) and a surface of intermediate work-function. Away from the surface, the atomic level lies below the Fermi energy and the atom neutralizes via the $|0\rangle \rightarrow |a; k\rangle$ path as shown in Fig. 8(a). Close to the surface the level is image shifted above the Fermi energy and probability flows back into the positive ion sector $|L, k\rangle$. On the outgoing leg of the trajectory, the atomic level shifts back below the Fermi energy and the atom again neutralizes by filling up $|a; L, k, q\rangle$ sector. As the image shift is a monotonic function of distance z , higher order sectors do not become populated significantly during the atom-surface collision, as this would require more than two level crossings. In the dynamical problem there is back flow of probability, manifested as a decrease in entropy along part of the outgoing trajectory as shown in Fig. 10. The decrease in entropy does not contradict the quantum generalization of the H-theorem as the Hamiltonian now depends explicitly on time. Even though the incoming Li^+ ion is completely neutralized during its encounter with the $W = 1.59$ eV surface, the probability for exciting an electron into one of the unoccupied levels above the Fermi energy is only 0.098 in the independent-particle approximation. Thus the probability for the creation of a particle-hole excitation is comparably small.

Two conclusions should be emphasized. First, the introduction of a coarse-grained entropy permits a quantitative understanding of the loss-of-memory process and elucidates the origin of irreversibility in charge-transfer. It also facilitates analysis of the $1/N$ expansion. Second, truncation of the Hilbert space at first order in $1/N$ in most instances suffices for the dynamical charge transfer problem as the probability flow does not significantly populate higher order sectors during the course of the atom-surface interaction. This conclusion is supported by the independent-particle

approximation which shows that less than one particle-hole pair is produced under typical conditions.

V. AUGER PROCESSES

We can take advantage of the newly added extension to the Hilbert space to include Auger charge transfer processes in addition to the resonant processes considered up until now. It has been a long standing question²³ whether or not Auger processes are of comparable importance to resonant charge transfer. We show here that at least at low surface work-functions, Auger transitions may be required to obtain an accurate description of experiments involving Lithium bombardment of Copper surfaces with alkali overlayers. The measured yield of excited neutral Li(2p) atoms grows at the very lowest work-functions when the incoming kinetic energy of the Li⁺ ion is 100 eV. At kinetic energies of 400 eV, however, this feature appears to be absent.⁸

In a typical Auger process an electron from one of the filled states below the Fermi energy of momentum q transfers non-resonantly into the atomic orbital a , while a second metal electron below ϵ_F of momentum k is promoted to a state of momentum L of higher energy. Within the truncated Hilbert space transitions with $L > k_F$ and $k, q < k_F$ couple the $|0\rangle$ sector to the $|a; L, k, q\rangle$ sector as shown in Fig. 11(a). Two other possible Auger processes are shown schematically in Fig. 11(b) and (c). In these cases one of the metal electrons hops onto the atomic orbital while the other remains below the Fermi level but fills up a hole which was already present. These transitions couple the neutral $|a; k\rangle$ sector to the negative $|k, q\rangle$ sector. Other Auger processes which we do not consider here include Auger de-excitation of the neutral atom and transitions between the $|L, q\rangle$ and $|a; k\rangle$ sectors.

It is straightforward to include new terms in the Hamiltonian Eq. (1) which correspond to these processes:

$$H^{Aug}(t) = \frac{1}{N} \sum_{L,k,q} V_{a;Lkq}^{A(1)}(z) \hat{P}_1 c_L^{\dagger\alpha} c_{k\alpha} c_a^{\dagger\beta} c_{q\beta} + \frac{1}{\sqrt{N}} \sum_{l,k,q} V_{0;l k q}^{A(2)}(z) \hat{P}_2 c_l^{\dagger\alpha} c_{k\alpha} c_0^{\dagger\beta} c_{q\beta} + H.c. \quad (22)$$

We use the same notation here as in Eq. (1) except that now the sum over momenta indices is restricted to states either above or below the Fermi energy, depending on whether the index is a capital or lower case letter. We have normalized the couplings $V^{A(1,2)}$ differently to account for the N species of spins. For Auger transitions $V^{A(2)}$ from the neutral $|a; l\rangle$ sector to the negative $|k, q\rangle$ sector, a pre-existing hole in the metal of momentum l and specific spin must be filled. This is not the case for Auger transitions $V^{A(1)}$ from a positive ion to a neutral atom which involve the creation of two new holes of any spin; hence, the matrix element must be reduced by an additional factor of $1/\sqrt{N}$ to make the $N \rightarrow \infty$ limit well defined. As we work in the restricted Hilbert space defined previously, projection onto singly and doubly occupied atomic sectors occurs automatically and we may drop the projection operators $\hat{P}_{1,2}$ in the following equations. Before we proceed further it is useful to separate the Auger Hamiltonian into symmetric and antisymmetric parts (with respect to interchange of the momenta indices k and q) to accord with Eq. (9). We also ignore the momentum dependence of the Auger matrix elements by setting $V_{a;l k q}^{A(1,2)}(z) = V_a^{A(1,2)}(z)$. This approximation, like the one already imposed on the resonant matrix elements, can easily be relaxed to incorporate more complicated momentum dependence. With this assumption, the antisymmetric part of $H^{Aug}(t)$ vanishes, and

$$H^{Aug}(t) = \frac{1}{N} \sum_{L,k>q} V_a^{A(1)}(z) (c_L^{\dagger\alpha} c_{k\alpha} c_a^{\dagger\beta} c_{q\beta} + c_L^{\dagger\alpha} c_{q\alpha} c_a^{\dagger\beta} c_{k\beta}) \\ + \frac{1}{\sqrt{N}} \sum_{l,k>q} V_0^{A(2)}(z) (c_l^{\dagger\alpha} c_{k\alpha} c_0^{\dagger\beta} c_{q\beta} + c_l^{\dagger\alpha} c_{q\alpha} c_0^{\dagger\beta} c_{k\beta}) + H.c. \quad (23)$$

Adding the Auger Hamiltonian to the resonant one, Eq. (1), and projecting the resulting Schrödinger equation onto each sector of the Hilbert space, we obtain the following terms to be added to the equations of motion Eq. (10):

$$i \frac{d}{dt} F = \dots + \sqrt{2(1-1/N)} \sum_{a; L, k>q} V_a^{A(1)*}(z) \exp\{-i[(\epsilon_L - \epsilon_k - \epsilon_q)t + \phi_a(t)]\} S_{a;Lkq} \\ i \frac{d}{dt} B_{a;l} = \dots - 2\delta_{a,0} \sqrt{1-1/N} \sum_{k>q} V_0^{A(2)*}(z) \exp\{i[(\epsilon_k + \epsilon_q - \epsilon_l - 2\epsilon_0^{(2)} - U)t + \phi_0(t)]\} D_{kq} \\ i \frac{d}{dt} E_{Lk} = \dots \\ i \frac{d}{dt} D_{kq} = \dots - 2\sqrt{1-1/N} \sum_l V_0^{A(2)}(z) \exp\{-i[(\epsilon_k + \epsilon_q - \epsilon_l - 2\epsilon_0^{(2)} - U)t + \phi_0(t)]\} B_{0;l}.$$

$$\begin{aligned}
i \frac{d}{dt} S_{a;Lkq} &= \dots + \sqrt{2(1-1/N)} V_a^{A(1)}(z) \exp\{i[(\epsilon_L - \epsilon_k - \epsilon_q)t + \phi_a(t)]\} F. \\
i \frac{d}{dt} A_{a;Lkq} &= \dots
\end{aligned} \tag{24}$$

Here the ellipses denote all of the terms in the original equations of motion, Eq. (10), which remain unchanged. Like Eq. (10), the new equations of motion, Eq. (24), are exact in the $N \rightarrow \infty$ limit. Higher order terms are suppressed by powers of $1/N$.

Before we proceed with the solution of the above system of equations, we must find reasonable values for the Auger matrix $V_a^{A(1,2)}(z)$. Adopting the same parametrization scheme for $V_a^{A(1,2)}(z)$ as in the case of the resonant couplings, we assume that the couplings fall off exponentially fast at large distances from the surface and saturate close to it. As now there are four overlapping wave functions in the matrix element (compared to two in the resonant case) we expect the coupling to fall off roughly twice as fast away from the surface²⁴. We obtain the couplings from the corresponding atomic half-widths by using the Fermi Golden Rule. For the neutral atom:

$$\Delta_a^{A(1)}(z) = \pi \sum_{k,q,L} |V_a^{A(1)}(z)|^2 \rho \delta_{\epsilon_L + \epsilon_a^{(1)} - \epsilon_k - \epsilon_q, 0}, \tag{25}$$

and for transitions to the negative ion state:

$$\Delta_0^{A(2)}(z) = \pi \sum_{k,q,l} |V_0^{A(2)}(z)|^2 \rho \delta_{\epsilon_0^{(1)} - \epsilon_l, 2\epsilon_0^{(2)} + U - \epsilon_k - \epsilon_q} \tag{26}$$

where again the density of states for a conduction band described by a set of M equidistant levels spaced D/M apart is given by $\rho = M/D$. From Eq. (25), it follows that:

$$\Delta_a^{A(1)}(z) = \frac{1}{2} \pi (M/D)^3 |V_a^{A(1)}(z)|^2 (\epsilon_a^{(1)} - \epsilon_F)^2 \theta(\epsilon_F - \epsilon_a^{(1)}). \tag{27}$$

In Eqs. (27) the Auger rate is proportional to $(\epsilon_a - \epsilon_F)^2$. The rate, like the inverse lifetime of a quasiparticle in a Landau Fermi liquid,²⁵ drops rapidly as the phase space available to particle-hole pair excitations decreases. For $|\epsilon_a^{(1)} - \epsilon_F| = D$, however,

$$\Delta_a^{A(1)}(z) = \frac{\pi}{2} \frac{M^3}{D} |V_a^{A(1)}(z)|^2. \tag{28}$$

Assuming that the holes are confined to the energies just below the Fermi level, and assuming that the energy difference between the negative ion state and the neutral ground state equals the half-bandwidth D , we also find:

$$\Delta_0^{A(2)}(z) = \frac{\pi}{2} \frac{M^3}{D} |V_0^{A(2)}(z)|^2. \tag{29}$$

To be concrete, we choose as trial parameters for $\Delta_a^{A(1,2)}$ those listed in Table II and obtain the matrix elements $V^{A(1,2)}$ from Eqs. (28) and (29). Of course, the matrix elements themselves, not the widths, are of fundamental importance in the many-body theory. For instance, the sign of the couplings is important; we choose $V^{A(1)} > 0$ and $V^{A(2)} < 0$ so that the Auger processes interfere constructively with the resonant ones. The Fermi Golden rule then determines the magnitude of the matrix elements in an approximately correct, but M -independent, way. The results of the dynamical calculation for Lithium which includes both resonant and Auger charge transfer are presented in Fig. 12. The Auger couplings have been chosen to be sufficiently small so that the peak in the excited neutral Li(2p) occupancy remains at work-function $W \approx 2.8$ eV. Now, however, there is a second upturn at $W \approx 1.5$ eV in qualitative agreement with experiment⁸. These features are robust as the two upturns remain even when the Auger rates are doubled or halved. To understand the origin of the second upturn at low work-functions, we first review the explanation for the existence of a peak at $W = 2.8$ eV when there is only resonant charge transfer⁸. Dynamical competition between Li(2p) and Li(2s) states is the key to understanding the photon peak. As the atom bounces away from the surface the coupling between the surface and the atom falls off faster for the Li(2s) state than for the Li(2p) state because the Li(2p) orbital is larger and of higher energy than the Li(2s) orbital. At the highest work function values, the energy of Li(2p) state lies above the Fermi level at all distances from the surface and is unoccupied. However, as the work-function is lowered, Li(2p) state begins to cross the Fermi level at closer distances where its coupling to the surface is appreciable while the coupling to Li(2s) is still small. For this intermediate range of work-functions, the Li(2p) state becomes populated on the outgoing leg of the trajectory despite the fact that it is

always energetically less favorable than Li(2s). As the work-function drops further, the Fermi level crossing for the Li(2p) state occurs at distances for which coupling to Li(2s) is appreciable. Now the Li(2p) state yields its occupancy to the lower energy Li(2s) state.

Consider what happens when the Auger coupling is turned on. At the very lowest work-functions, Auger transitions between the Li(2p) state and the metal occur more frequently because the phase space for these processes grows rapidly as $(\epsilon_a^{(1)} - \epsilon_F)^2$ increases. As we expect the $\Delta_{2s}(z)$ Auger rate to fall off more rapidly away from the surface than the $\Delta_{2p}(z)$ Auger rate, the picture outlined above in the resonant case simply repeats itself and there is a second upturn in Li(2p) occupancy. However, as evident from Fig. 12, the second rise in Li(2p) occupancy is not noticeable at the higher incoming kinetic energy of 400 eV. In the 100 eV case the atom moves only half as fast as in 400 eV case and there is sufficient time for an electron to make an Auger transition to the excited neutral Li(2p) state. At higher velocities there is not enough time for an Auger transition to occur.

While the model developed here reproduces the upturn in the excited neutral Li(2p) occupancy at the very lowest work-functions, it is only one of several possible explanations for the feature. Two difficulties impede further progress. Experimentally, it is hard to measure absolute yields of ejected Auger electrons. Relative yields, as measured in Auger spectroscopy²⁶, provide little guidance. Most of the Auger electrons are promoted to unoccupied metal states instead of ejected from the surface. Indirect probes, such as the formation of excited states, appear to be the only way to gauge the relative importance of Auger processes. Theoretically, Auger matrix elements cannot be computed accurately because Auger transitions are driven by many-body correlations²⁷. The parameters for the Auger rates listed in Table II are at best just an educated guess. Indeed, calculations to date have focused on Auger widths as opposed to matrix elements which are of more fundamental importance. Either constructive or destructive interference with resonant processes is possible, but only a full microscopic calculation of both types of matrix elements can determine the relative sign.

VI. CONCLUSIONS

In this paper we described a generalized Newns-Anderson model of charge transfer and its systematic solution based on a $1/N$ expansion. We went beyond earlier work by including new sectors in the Hilbert space and showed that loss-of-memory was improved. We analyzed the effect of the truncation of the Hilbert space on loss-of-memory by studying entropy production both within the approximate solution to the many-body theory and also within the independent-particle approximation. This analysis showed how the $1/N$ truncation scheme works in dynamical problems. In most cases, higher order sectors can be neglected as less than one particle-hole pair is produced during the atom-surface collision. This conclusion was supported by the independent-particle approximation. Despite the fact that an unlimited number of particle-hole pairs can be accommodated within this approximation, typically less than one is created during an atom-surface interaction. The production of entropy during the collision demonstrates the irreversibility of the interaction: at velocities of experimental interest, information about the initial state of the incoming atom is dissipated.

We included Auger processes and showed that an experimentally observed upturn in photon yield due to the formation of excited Li(2p) atoms at the very lowest work-functions can be explained in terms of competition between the Li(2s) and Li(2p) states and the rapid growth at low work-functions in the phase space for Auger transitions. Finally, we examined whether Kondo effects are experimentally accessible, and concluded that it will be extremely difficult to separate the small predicted effects from other, more mundane, nonlinearities.

VII. ACKNOWLEDGMENTS

We thank Ernie Behringer, Dennis Clougherty, Barbara Cooper, Dan Cox, David Goodstein, Peter Nordlander, Hongxiao Shao, Chris Weare, and especially Eric Dahl for fruitful discussions. This work was supported in part by the National Science Foundation through Grants Nos. DMR-9313856 and DMR-9357613 and by a grant from the Alfred P. Sloan Foundation.

¹ J.B. Marston et.al., Phys. Rev. B **48**, 7809 (1993).

- ² C. M. Varma and Y. Yafet, Phys. Rev. B **13**, 2950 (1976). See also: O. Gunnarsson and K. Schönhammer, Phys. Rev. B **28**, 4315 (1983).
- ³ R. Brako and D. M. Newns, Solid State Commun. **55**, 633 (1985).
- ⁴ D. R. Andersson, E. R. Behringer, B. H. Cooper, and J. B. Marston, *Journal of Vacuum Science and Technology* **A11(4)**, 2133 – 2137 (1993); E. R. Behringer, D. R. Andersson, B. Kasemo, B. H. Cooper, and J. B. Marston, *Nuclear Instruments and Methods in Physics Research* **B78**, 3 – 10 (1993).
- ⁵ C. B. Weare and J. A. Yarmoff, “Resonant Neutralization of ${}^7\text{Li}^+$ Scattered from Alkali/Al(110) as a Probe of the Local Electrostatic Potential,” submitted to Surf. Sci.
- ⁶ J. Hermann et al., Surf. Sci. **138**, 570 (1984); B. Hird *et al.*, Phys. Rev. Lett. **67**, 3375 (1991).
- ⁷ J. Los and J. J. C. Geerlings, Phys. Reports **190**, 133 (1990).
- ⁸ E.R. Behringer, D.R. Andersson, B.H. Cooper and J.B. Marston, unpublished.
- ⁹ H.-J. Kwon, A. Houghton, and J. B. Marston, Phys. Rev. B **52**, 8002 (1995).
- ¹⁰ P. Nordlander and J. C. Tully, Phys. Rev. Lett. **61**, 990 (1988); Surf. Sci. **211/212**, 207 (1989); Phys. Rev. B **42**, 5564 (1990).
- ¹¹ P. Nordlander, Phys. Rev. B **46**, 2584 (1992).
- ¹² Ernest Behringer, *The Dynamics of Resonant Charge Transfer In Hyperthermal Energy Ion-Surface Collisions* (Ph.D. thesis, Cornell University, 1994)
- ¹³ R. Brako and D. M. Newns, Surf. Sci. **108**, 253 (1981).
- ¹⁴ To obtain a copy of the computer programs “next.c” and “single.c” contact J. B. Marston.
- ¹⁵ Hongxiao Shao, Peter Nordlander, and David C. Langreth, Phys. Rev. B **52**, 2488 (1995).
- ¹⁶ Peter Nordlander, Hongxiao Shao, and David C. Langreth, Phys. Rev. B **49**, 13929 (1994) and Phys. Rev. B **49**, 13948 (1994).
- ¹⁷ A. C. Hewson, *The Kondo Problem to Heavy Fermions* (Cambridge University Press, New York, 1993) p. 211.
- ¹⁸ T. A. Costi, J. Kroha, and P. Wölfle, “Spectral Properties of the Anderson Impurity Model: Comparison of Numerical Renormalization Group and Non-Crossing Approximation,” cond-mat/9507008, unpublished.
- ¹⁹ R. Brako and D. M. Newns, Rep. Prog. Phys. **52**, 655 (1989).
- ²⁰ E. Dahl, unpublished.
- ²¹ P.C.W. Davies, *The Physics of Time Asymmetry* (University of California Press, Berkeley, 1974) pp. 157 – 160.
- ²² L.D. Landau and E. Lifshitz, *Statistical Physics, Part I* (Pergamon Press, Oxford, 1980).
- ²³ A.T. Amos, B.L. Burrows, S.G. Davison, Surf. Sci. Lett. **277**, 100 (1992).
- ²⁴ Tony Fonden and Andre Zwartkruis, Surf. Sci. **269/270**, 601 (1992).
- ²⁵ John W. Negele and Henri Orland, *Quantum Many-Particle Systems* (Addison-Wesley Publishing Company, Redwood City, California, 1988) p. 254.
- ²⁶ H. Schall, H. Brenten, K. H. Knorr, and V. Kempter, Z. Phys. D **16**, 161 (1990); H. Brenten *et al.*, Surf. Sci. **243**, 309 (1991); Nucl. Instrum. Methods B **58**, 328 (1991).
- ²⁷ N. Lorente and R. Monreal, Nucl. Instrum. Methods Phys. Res. B **78**, 44 (1993); R. Monreal and N. Lorente, “Dynamical screening in Auger processes near metal surfaces,” unpublished.

TABLE I. Parameters appearing in Eq. 6 which characterize the resonant half-widths for different atomic states of Lithium. All parameters are in atomic units.

ATOMIC STATE	Δ_0	α	Δ_{sat}
$Li^0(2s)$	2.23	0.86	0.04
$Li^0(2p_z)$	0.70	0.54	0.04
$Li^-(2s^2)$	0.18	0.38	0.05

TABLE II. Parameters which characterize the Auger half-widths for Lithium. All parameters are in atomic units.

ATOMIC STATE	Δ_0	α	Δ_{sat}
$Li^0(2s)$	14	1.8	0.7
$Li^0(2p_z)$	10	1.3	0.6
$Li^-(2s^2)$	5	1.4	0.3

FIG. 1. Schematic of the different sectors of the Hilbert space up to order $1/N$. The new sector is highlighted in the box. Still missing at $O(1/N)$ are amplitudes for a negative ion with two holes plus a particle-hole pair in the metal.

FIG. 2. Resonant charge transfer couples the different sectors of the truncated Hilbert space indicated by the arrows.

FIG. 3. The measured and predicted normalized yields of the excited neutral atom Li(2p) (triangles) versus the surface work-function W . In the experiment, Li^+ is incident on K/Cu(001) with initial kinetic energy $E_0 = 400$ eV. The peak occurs at $W \approx 2.8$ eV. Solid and the dashed lines are the results of the improved approximate solution of the many-body model ($N = 2$) for two different initial conditions. In this case the band consists of $M = 30$ states above and 30 states below the Fermi surface with a half-bandwidth of $D = 4$ eV. The atomic level width parameters are given in Table I. For the initial condition of the equilibrium ground state (solid line) the trajectory begins from the point of closest approach ($z_0 = 1.0\text{\AA}$) with an outward velocity given by $u_f = 0.03$ a.u. For the initial condition of a neutral atom (dashed line), the trajectory starts at $z_f = 20.0\text{\AA}$ with initial velocity of $u_i = 0.04$ a.u., bounces at $z_0 = 1.0\text{\AA}$, and leaves the surface with a lower outward velocity of $u_f = 0.03$ a.u. The experimental and theoretical yields, which agree in magnitude, are here normalized to unity. We attribute the broader width of the experimental peak to inhomogeneities in the surface potential due to the K adsorbates.

FIG. 4. (a) The calculated neutralization probability for Lithium ($N = 2$) as a function of outgoing velocity u_f using the improved approximate solution. Three different initial conditions are examined. The incoming velocity, except in the case of the ground state initial condition, is given by $u_i = (4/3)u_f$. The surface work-function is $W = 4.59$ eV, corresponding to a clean Cu(001) surface. (b) Same as (a) but using the smaller variational Hilbert space and equations of motion of [I].

FIG. 5. The occupancies of the different charge states A^+ , A^0 and A^- as a function of time for *fixed* atomic position $z = z_0$. A Lithium atom ($N = 2$) interacts with a metal surface of work-function $W = 4.59$. Time evolution begins from each of the following four initial conditions: (a) Positive ion A^+ at $z = 1\text{\AA}$. The final occupancies (at $t = 8.2 \times 10^{-15}$ sec.) are $P^+ = 0.7806$, $P^0 = 0.2134$ and $P^- = 0.0058$. (b) Neutral atom A^0 at $z = 1\text{\AA}$. The final occupancies are $P^+ = 0.7471$, $P^0 = 0.2480$ and $P^- = 0.0047$. (c) Negative ion A^- at $z = 1\text{\AA}$. The final occupancies are $P^+ = 0.028$, $P^0 = 0.9508$ and $P^- = 0.0204$. (d) Equilibrium ground state at $z = 1\text{\AA}$. The final occupancies are $P^+ = 0.7965$, $P^0 = 0.1983$ and $P^- = 0.0071$.

FIG. 6. Time-evolution of the dimensionless coarse-grained entropy $S_{cg}(t)$ for a *fixed* atomic position $z = 1\text{\AA}$. Initially, at $t = 0$, the Lithium atom is a positive ion. It then interacts with a metal surface of work-function $W = 1.59$. The independent-particle and the two approximate many-body solutions are compared for the case of spinless electrons, $N = 1$.

FIG. 7. Coarse-grained entropy $S_{cg}(t)$ as a function of time for the approximate many-body solution in the physical case $N = 2$ for a *fixed* atomic position $z = 1\text{\AA}$ and a surface work-function of $W = 4.59$ eV. Three different initial conditions are studied.

FIG. 8. Schematic showing the different sectors of the Hilbert space up to order $1/N$. The arrows indicate the direction of probability flow as the entropy grows. In (a), coupling to the negative ion A^- is turned off and the corresponding sector is not shown. In (b) all sectors discussed in the paper are shown plus an A^+ sector at second order in $1/N$ which has not been included. We conjecture that loss-of-memory from an initial A^- state would occur if the Hilbert space were expanded further to include this sector.

FIG. 9. Occupancies as a function of time for a *fixed* atomic position $z = 1\text{\AA}$. The pure initial state is a positive ion (A^+) which then decays. For clarity, the coupling to the negative ion and excited neutral sectors is turned off. (a) The surface work-function is $W = 1.59$ eV. (b) Same as (a) except the surface work-function is $W = 3.28$ eV. In both (a) and (b) a cascade of probability flow from the low-order to the higher-order sectors of the Hilbert space is evident.

FIG. 10. Time-evolution of the dimensionless entropy $S_{cg}[z(t)]$ in the full dynamical problem for spinless fermions ($N = 1$). We compare the independent-particle solution with the many-body solution; only the coupling to the Li(2s) state is turned on. A positive Lithium ion with an incoming velocity of $u_i = 0.04$ a.u. interacts with a metal surface of work-function $W = 1.59$ eV. The atom bounces off the surface with an outgoing velocity of $u_f = 0.03$ a.u. and is completely neutralized. Note the comparable sizes of the two entropies. In this case, the probability for an electron to be excited into a state above the Fermi energy is only 0.098; hence the probability for the formation of a particle-hole pair is also small.

FIG. 11. Schematic of three different Auger processes. (a) A metal electron from below the Fermi level of momentum k transfers non-resonantly to the atomic orbital a while another electron from below the Fermi level of momentum q is promoted to a state of momentum L above the Fermi level to conserve energy. Final state transitions are possible only when the atomic level dips below the Fermi level, $\epsilon_a < \epsilon_F$. (b) and (c) Two other Auger processes which involve the negative ion. A metal electron from below the Fermi level transfers non-resonantly to the atomic orbital a , while another electron from below the Fermi level of momentum k jumps to a state of momentum l which is also below the Fermi level. Final state transitions in this case are possible both for (b) $\epsilon_a > \epsilon_F$ and for (c) $\epsilon_a < \epsilon_F$.

FIG. 12. The experimentally observed and theoretically predicted yield of excited neutral Li⁰(2p). In the experiment, an incident Li⁺ ion interacts with a metal surface of variable work-function. In the theory, $N = 2$, $M = 30$, and parameters which define the level widths due to Auger transitions are given in Table II. The initial condition in this case is (4), the equilibrium ground state at point of closest approach, though similar curves are also obtained for initial condition (2), the neutral atom far away. The solid line is for the case of $u_f = 0.03$ a.u. corresponding to an incoming kinetic energy of 400 eV. The dashed line corresponds to $u_f = 0.015$ a.u. or 100 eV. Yields are normalized to one.

Fig. 1

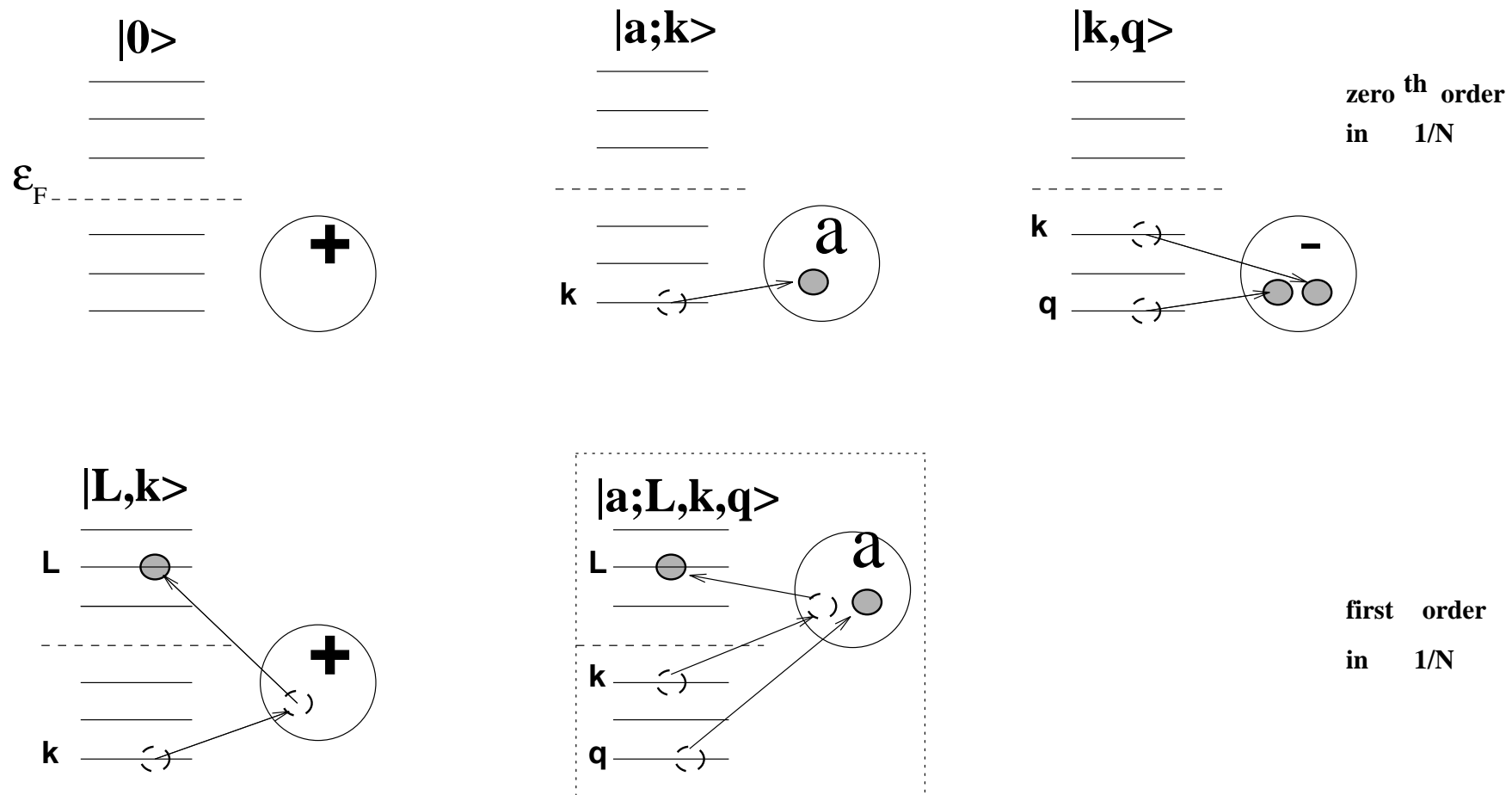


Fig. 2

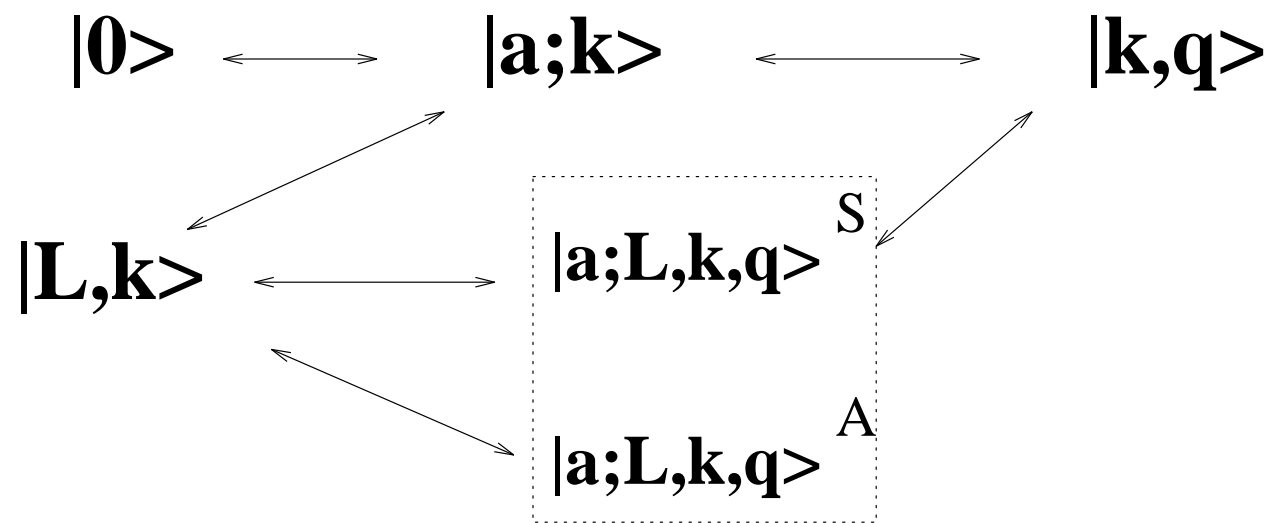


Fig. 3

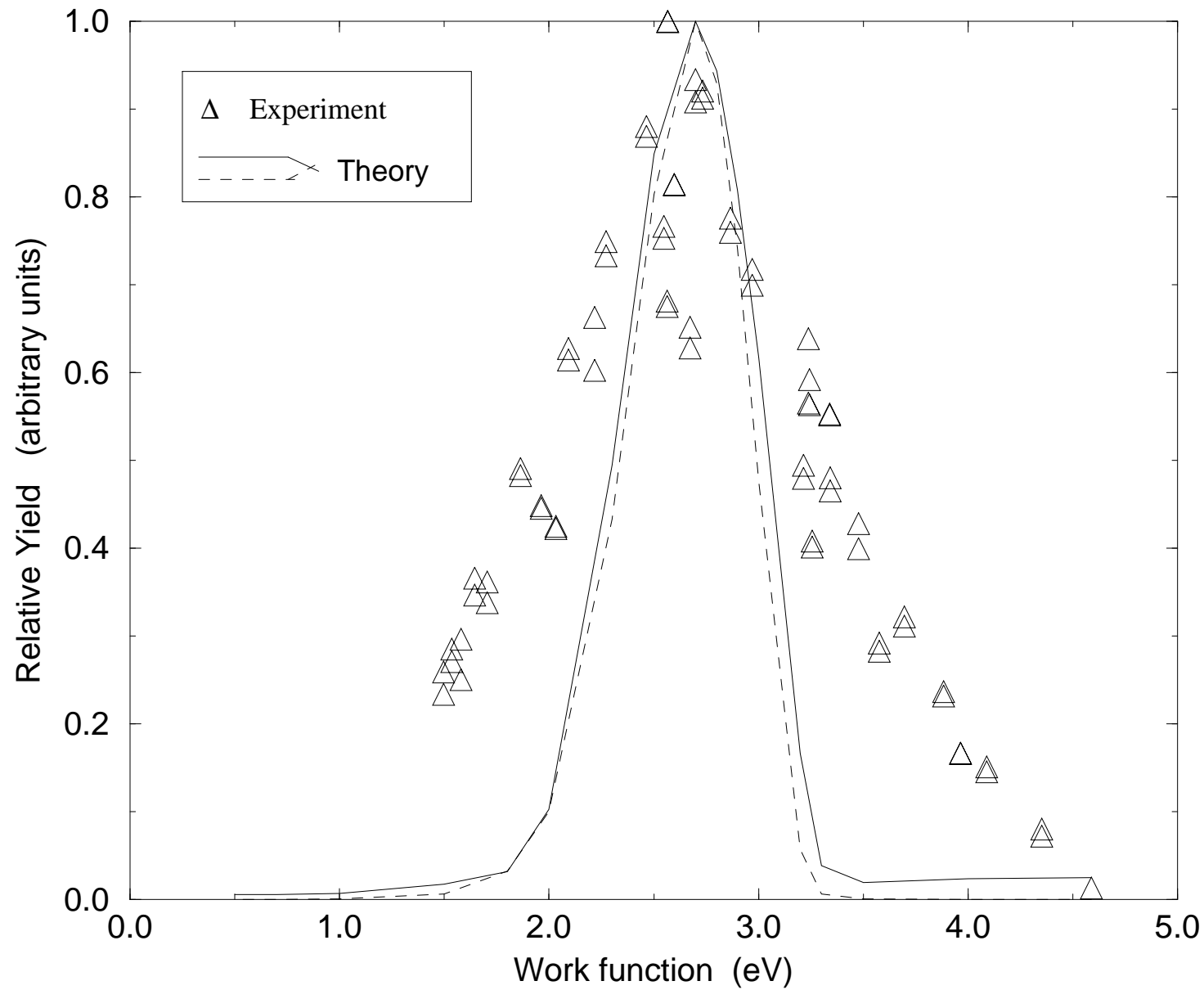


Fig. 4(a)

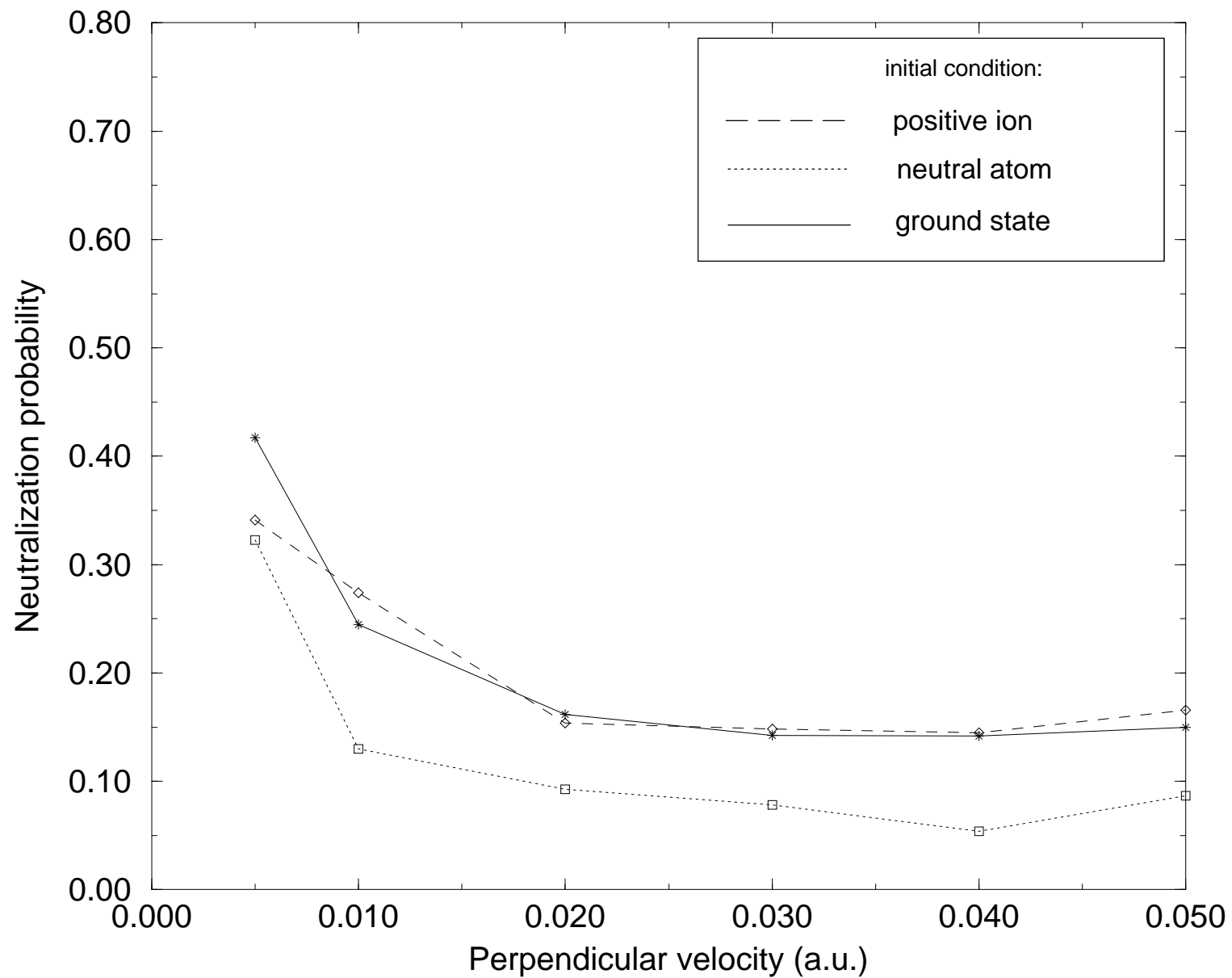


Fig. 4(b)

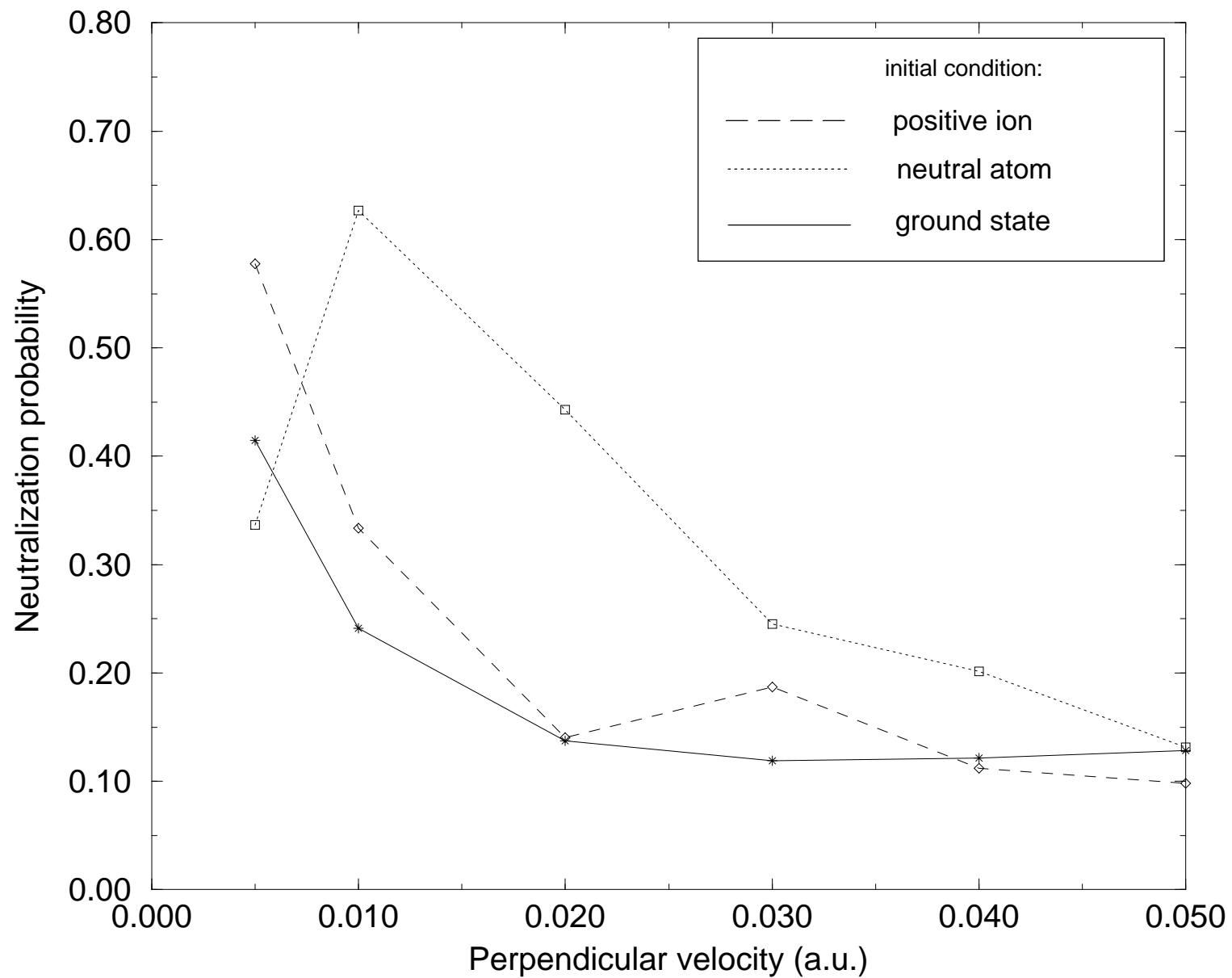


Fig. 5(a)

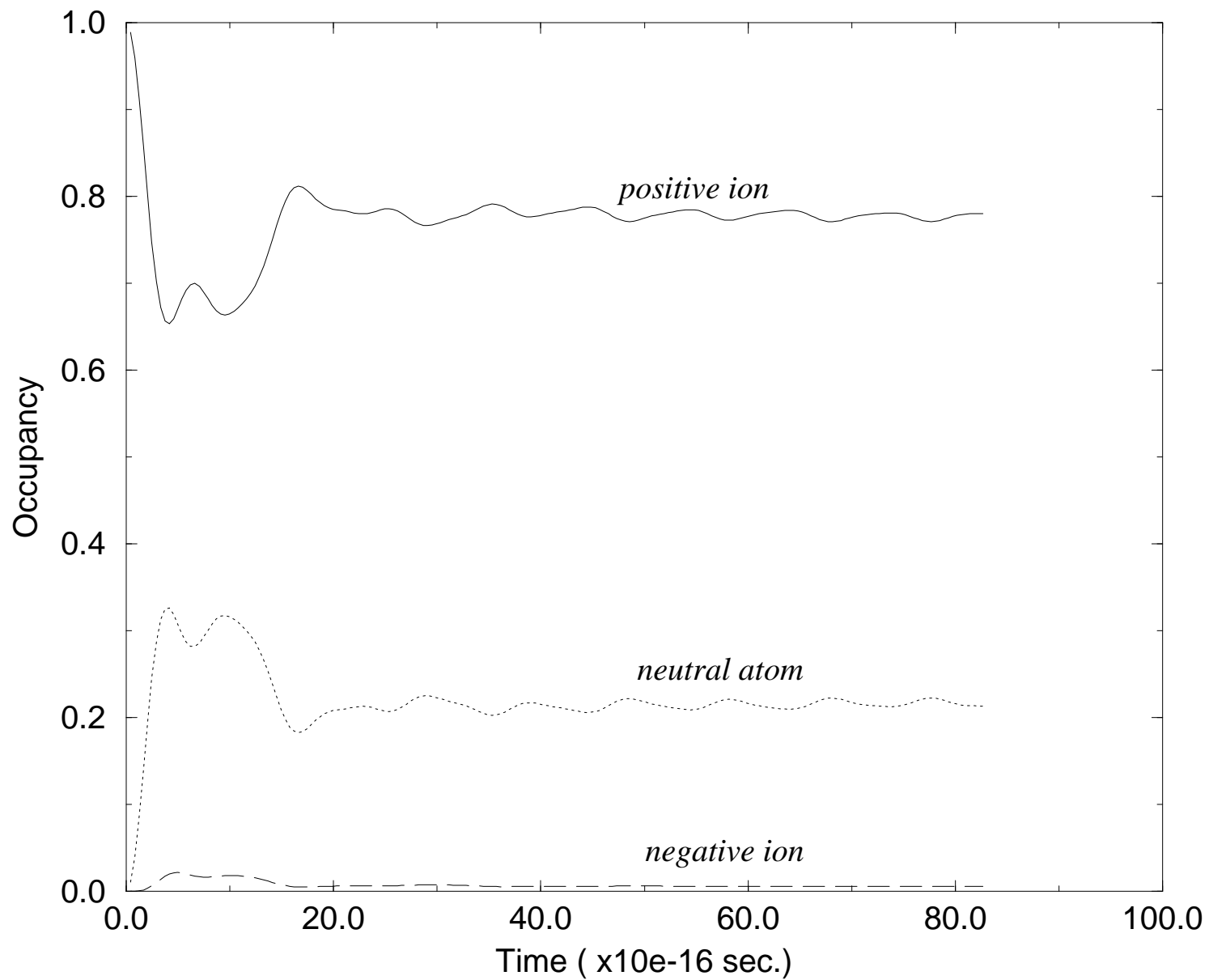


Fig. 5(b)

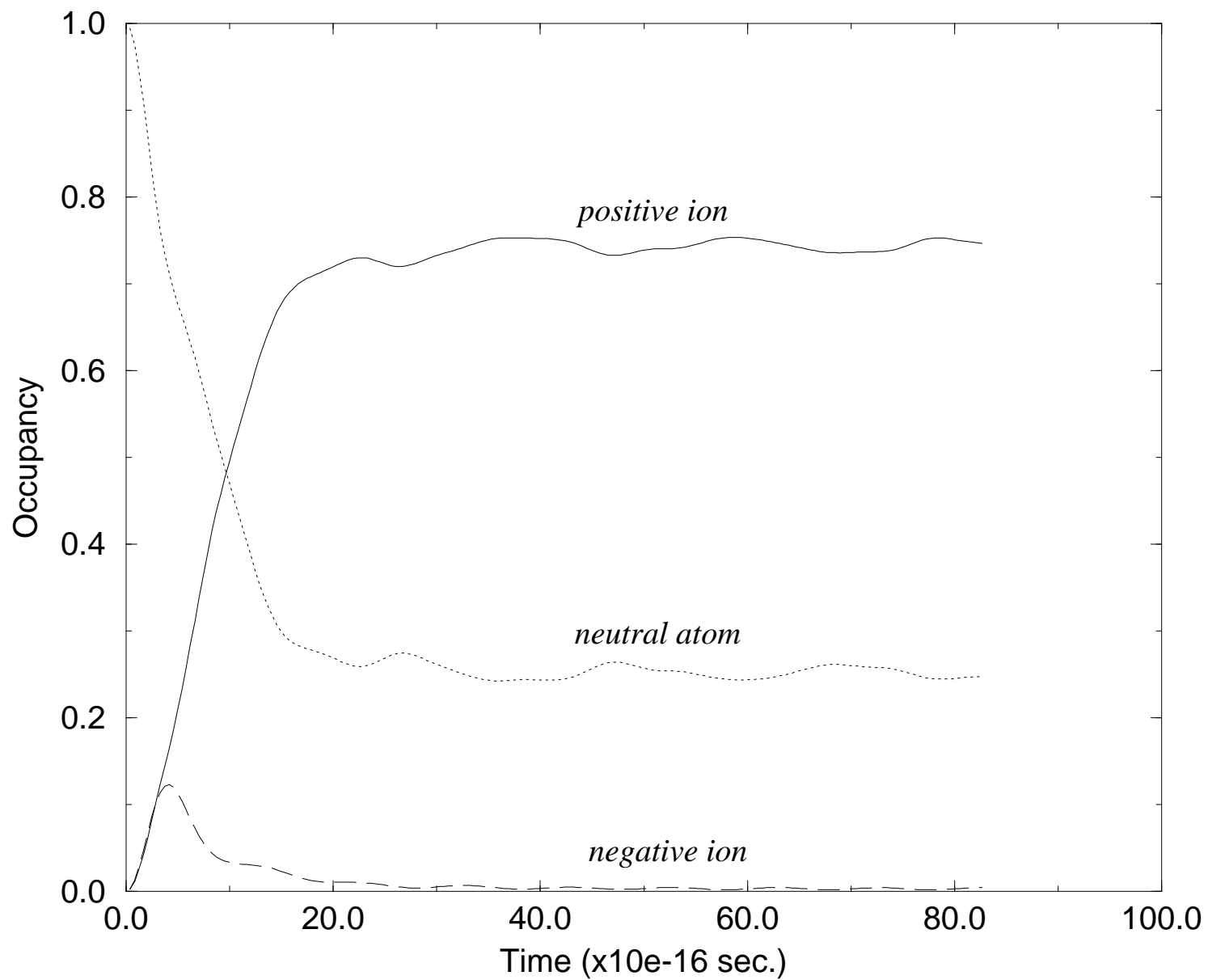


Fig. 5(c)

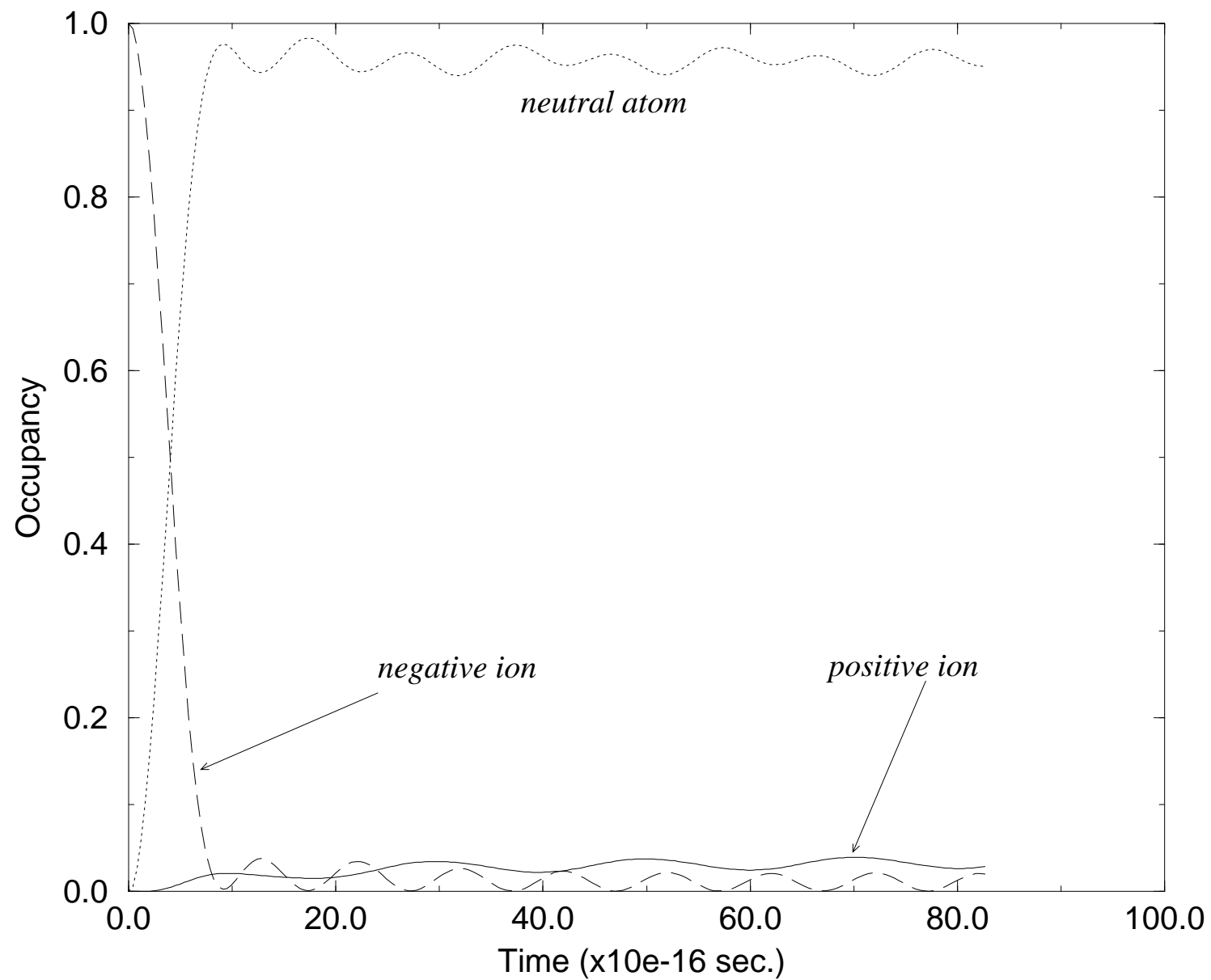


Fig. 5(d)

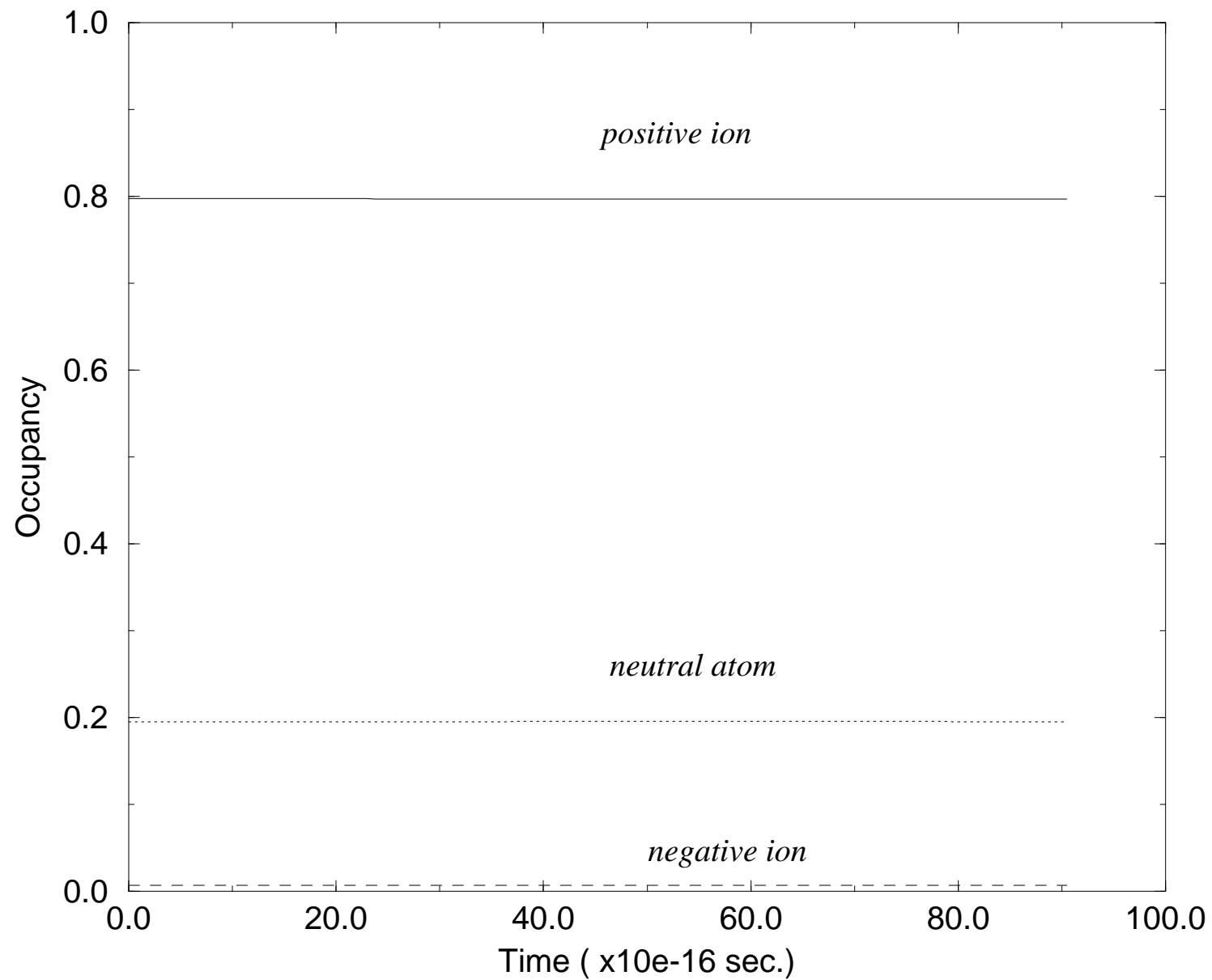


Fig. 6

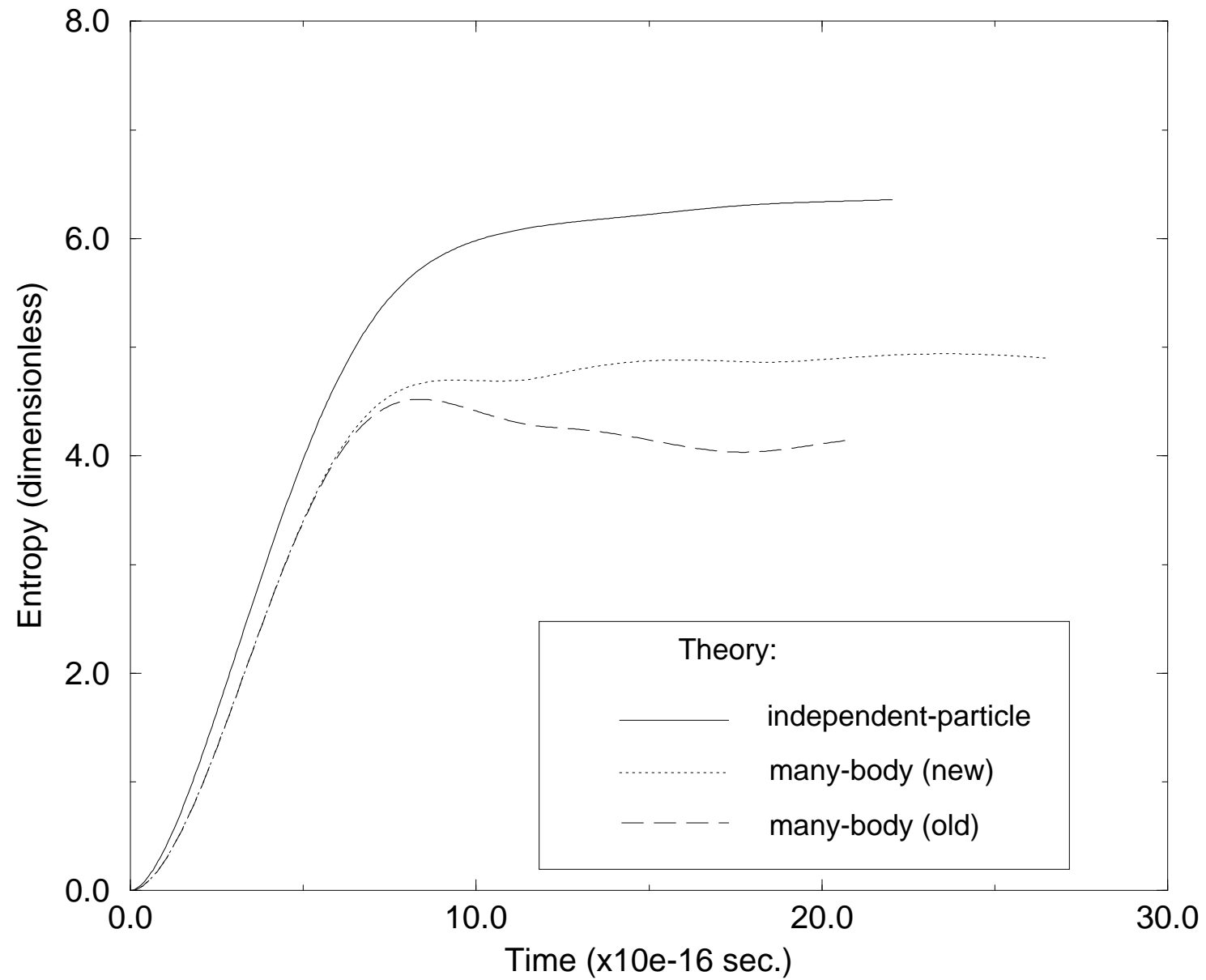


Fig. 7

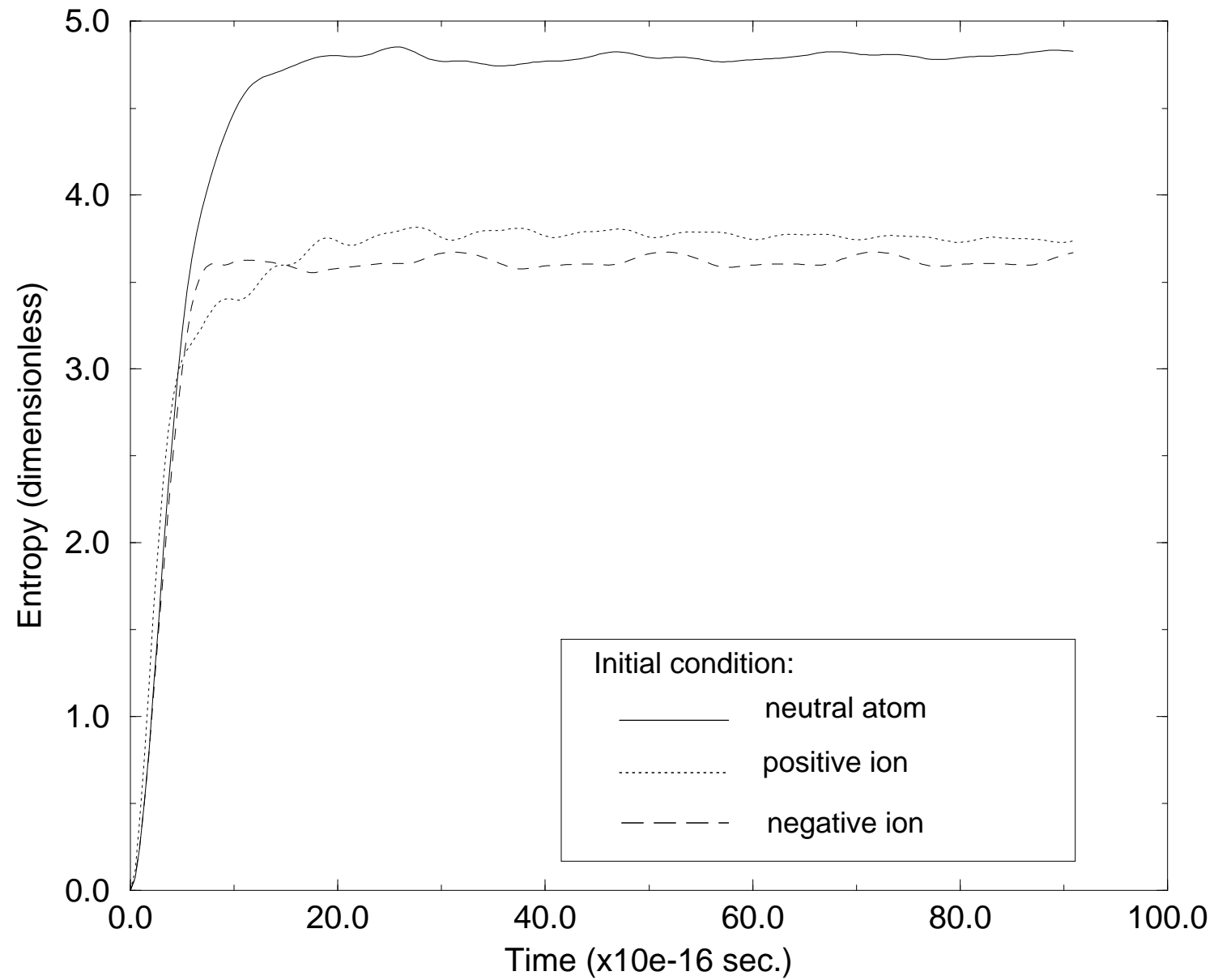


Fig. 8(a)

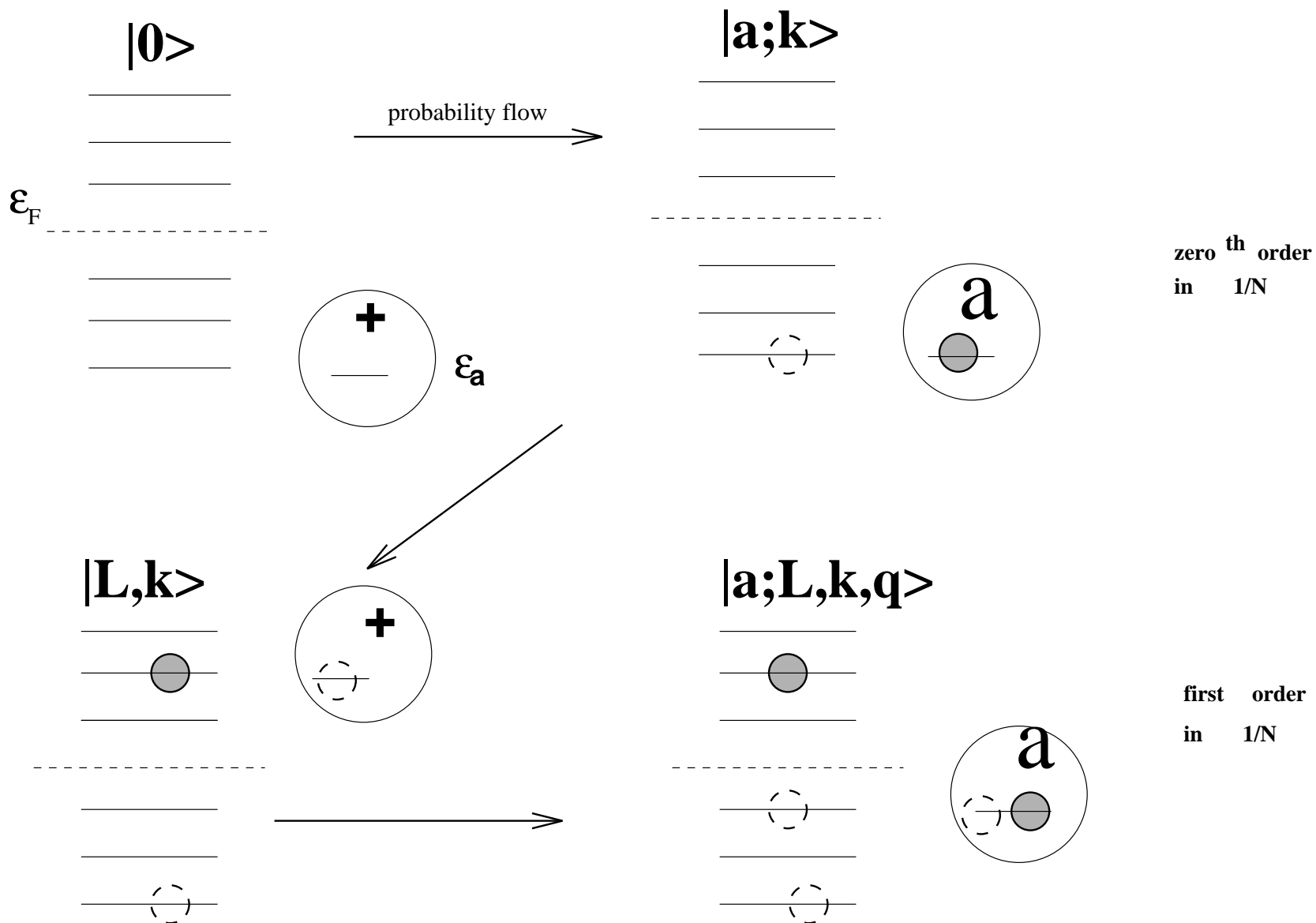


Fig. 8(b)

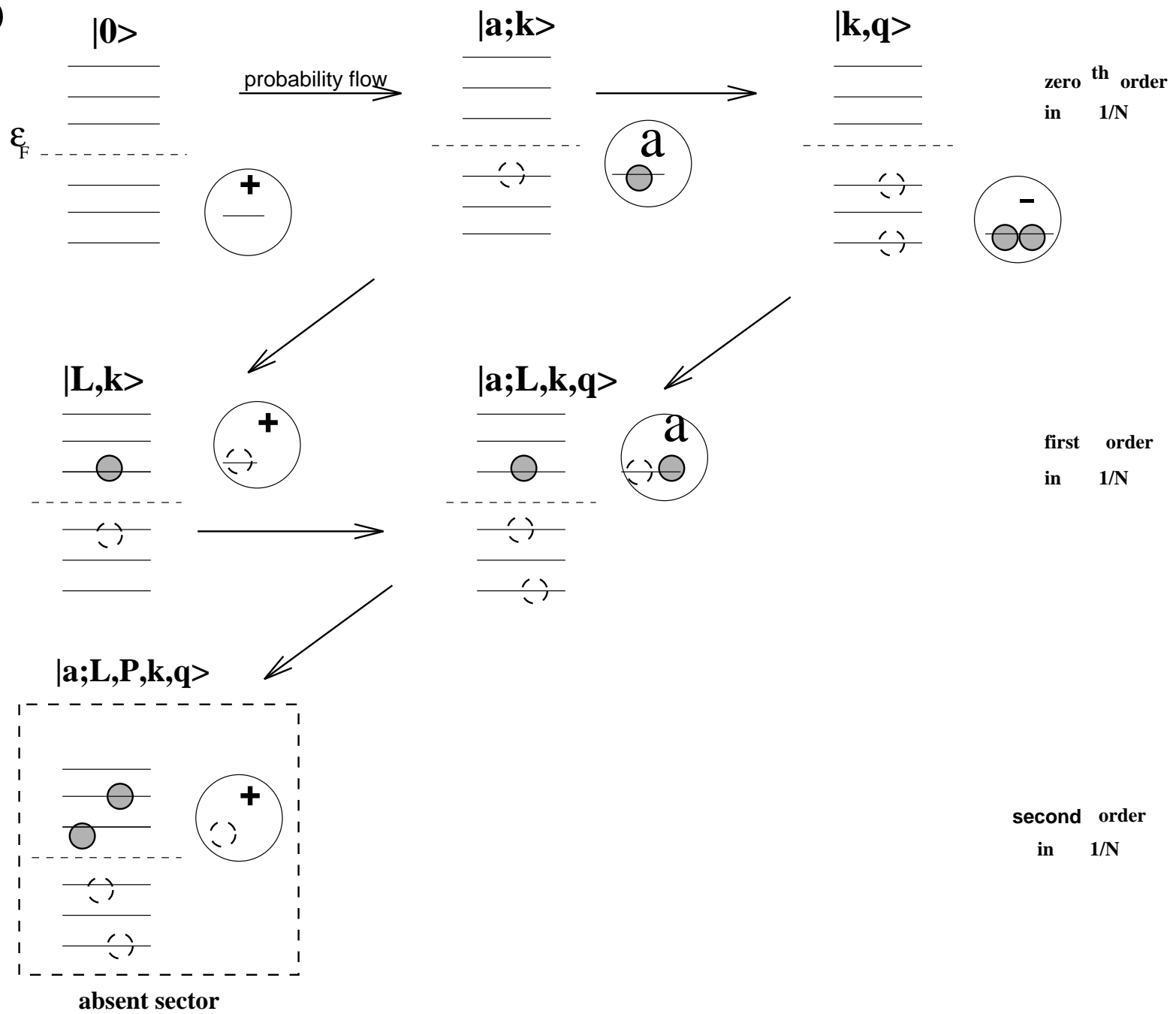


Fig. 9 (a)

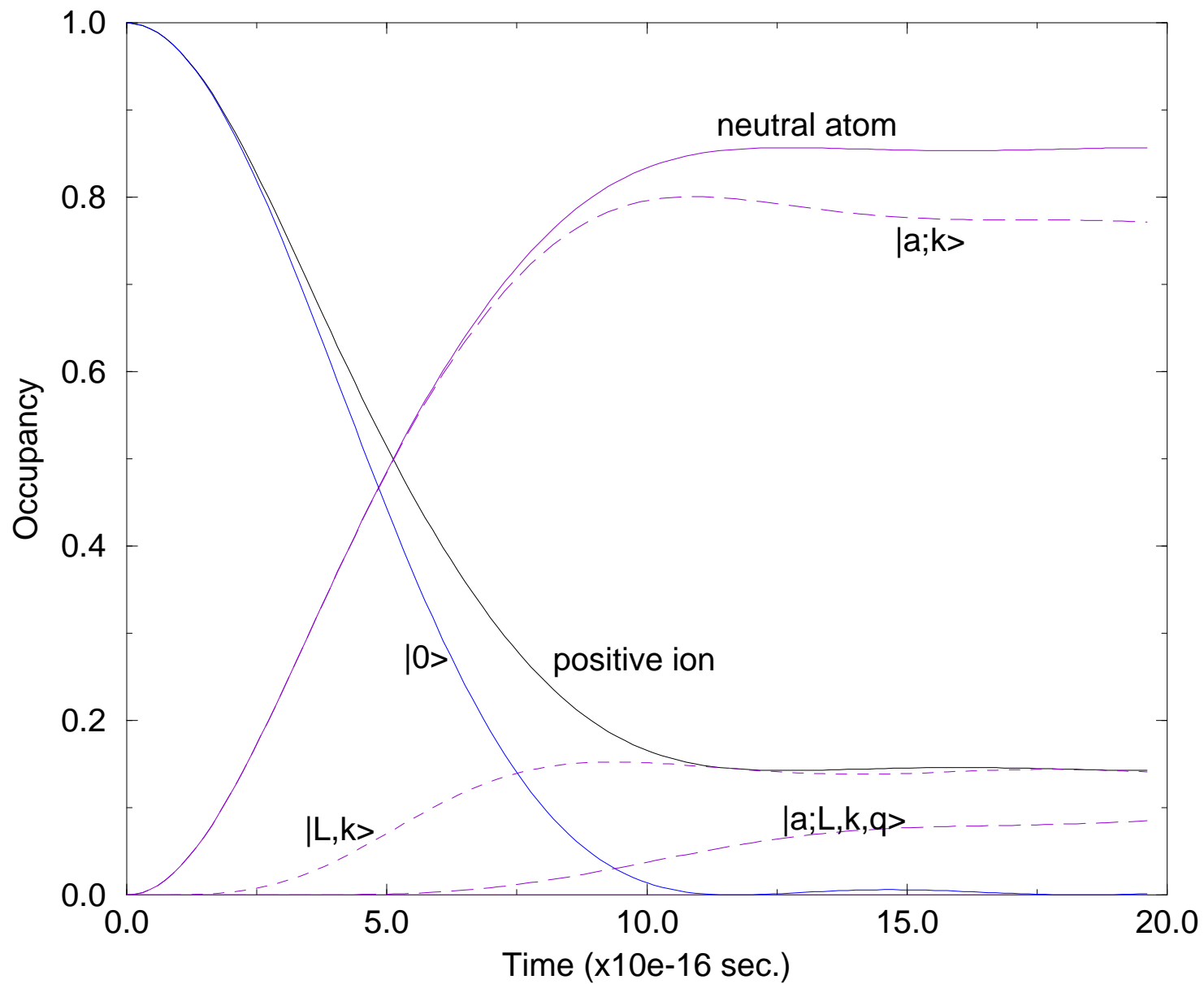


Fig. 9(b)

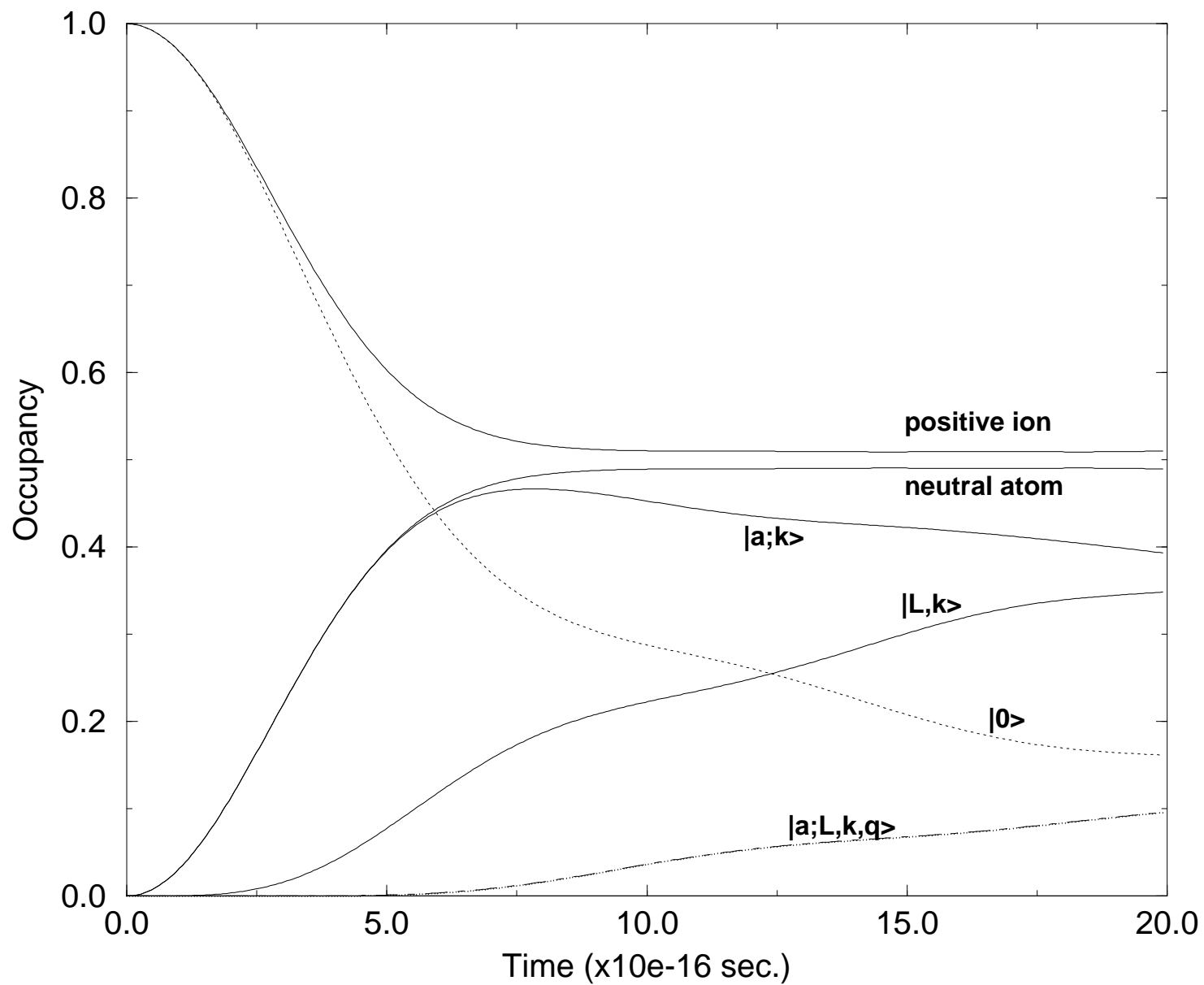


Fig. 10

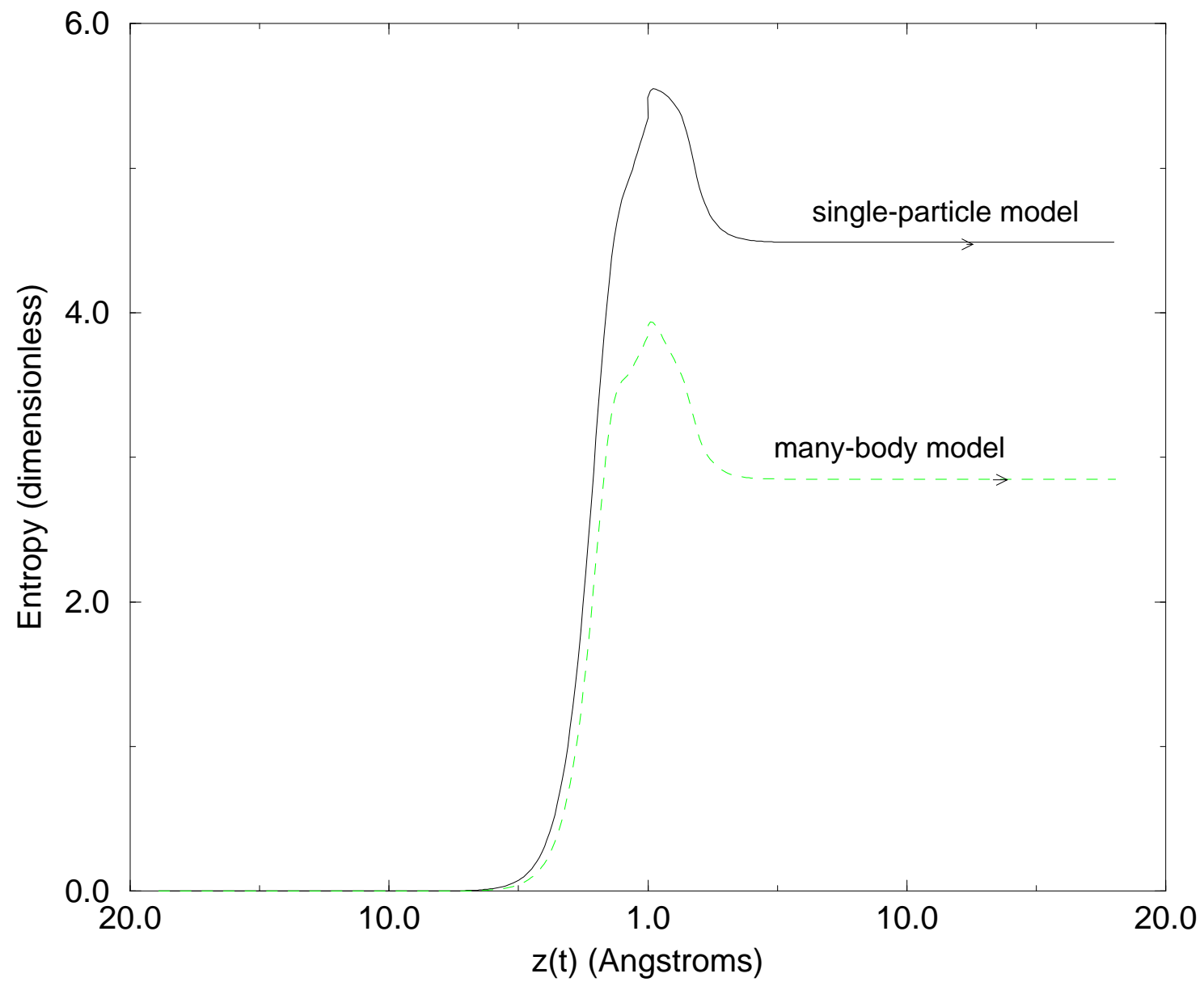


Fig. 11

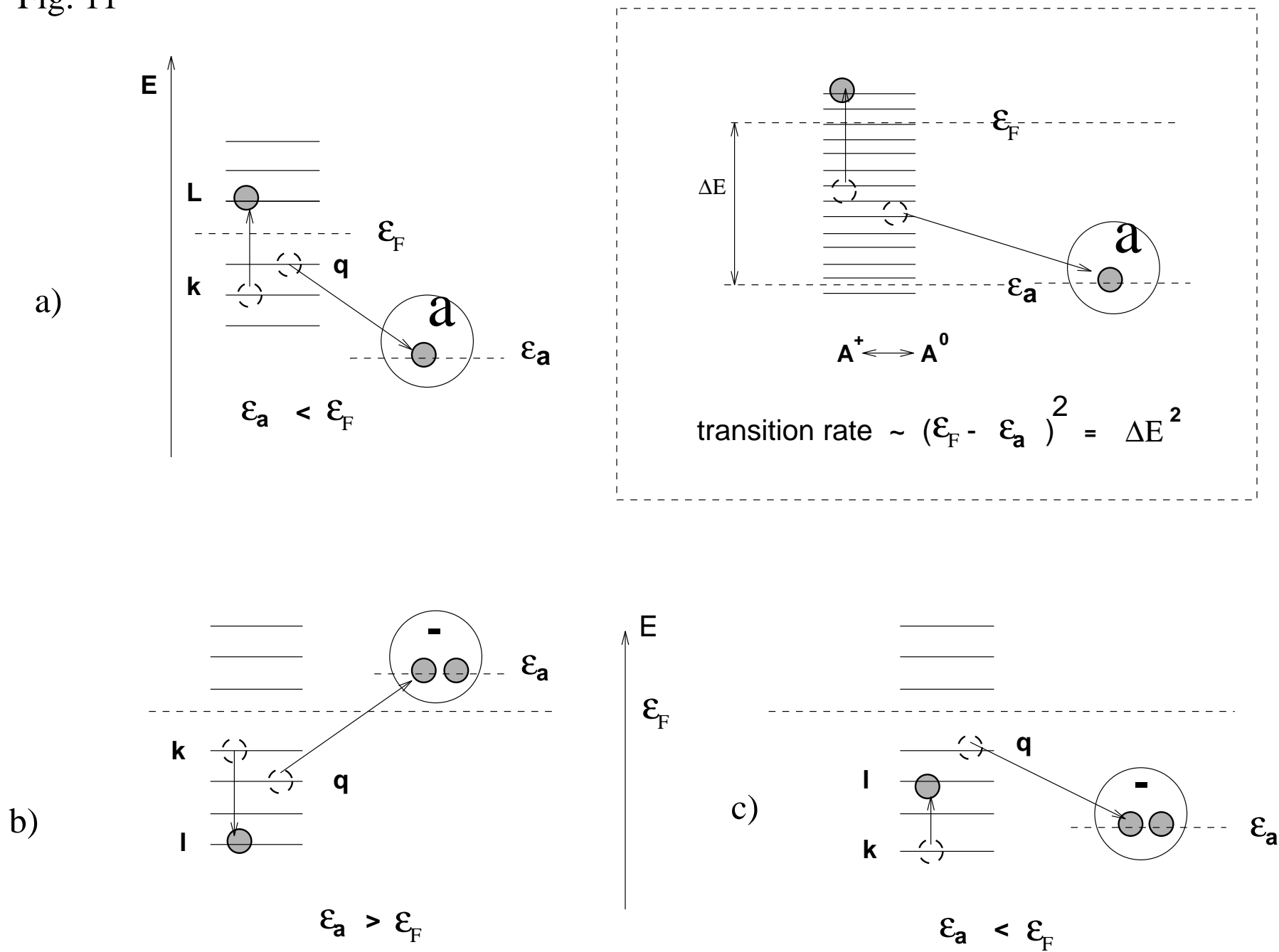


Fig. 12

